Geomorphological, stratigraphic and geochronological evidence of fast Pleistocene coastal uplift in the westernmost part of the Corinth Gulf Rift (Greece)

N. Palyvos [(1)(*)], M. Mancini [(2)], D. Sorel [(3)], F. Lemeille [(4)], D. Pantosti [(1)], R. Julia [(5)], M. Triantaphyllou [(6)], P.-M. DeMartini [(1)]

(1) Istituto Nazionale di Geofisica e Vulcanologia, Sez. Sismologia e Tettonofisica, Active Tectonics Group, pantosti@ingv.it, demartini@ingv.it

(*) now at Harokopio University, Geography Department, palyvos@hua.gr

(2) CNR, Istituto di Geologia Ambientale e Geoingegneria, Area della Ricerca Roma 1, via Salaria km 29.3, C.P. 10, 00016 Monterotondo Scalo, Roma, Italy, marco.mancini@igag.cnr.it

(3) Université Paris-Sud, Centre d'Orsay, Faculty of Geology, 91405 Orsay Cedex, sorel@geol.u-psud.fr

(4) Institut de Radioprotection et de Surete Nucléaire, Seismic Hazard Division, Fontenay-aux-roses Cedex, francis.lemeille@irsn.fr

(5) Institute of Earth Sciences Jaume Almera, Barcelona 08028, ramon.julia@ija.csic.es

(6) National and Kapodistrian University of Athens, Faculty of Geology and Geoenvironment, Department of Hist. Geology - Paleontology, mtriant@geol.uoa.gr

Abstract

Rapid extension and active normal faulting in the western extremity of the Gulf of Corinth are accompanied by intense coastal uplift. We investigate Pleistocene uplift west of Aigion, based on remains of marine coastal terraces and sedimentary sequences that we attempt to date by calcareous nannoplankton and U-series analyses. Initiation of net uplift in the study area was recent, caused by abandonment of an older rift-bounding normal fault zone and take-over by the presently active, coastal one. Take-over apparently coincides with an abrupt slow-down (or, termination) of secondary fault block tilting within the broader hangingwall block of the older zone, indicated by an angular unconformity that dates in the early part of MIS10 (~390-350 ka BP, preferably, in the earlier part of this period), based on nannoplankton and sequence-stratigraphic constraints. Net uplift driven by the coastal zone resulted in the formation of MIS9c (330 ka) and younger terraces. The formation of the unconformity and the initiation of net uplift, coincide temporally with a ~300-400 ka unconformity recognised by recent offshore studies in a wide area offshore Aigion. I.e., they could be part of an evolutionary event that affected the entire western part of the Corinth Rift or, a large area therein. Uplift rate estimates at four locations are discussed with reference to the morphotectonic context of differential uplift of secondary fault blocks, and the context of possible increase of uplift rate with time.

The most conservative and most useful estimate for uplift rate at the longitude of the studied transect is 1.74-1.85 mm/yr (based on nannoplankton). Because it refers to a location 3.8 km away from the coastal fault zone, it expectedly underestimates slightly the uplift rate that would be theoretically observed in its immediate footwall block area, if this area hadn't been collapsing via secondary faulting. Being a time-averaged estimate of uplift rate since MIS7e, it encompasses periods close to the initiation of net uplift, i.e. uplift rate could be slightly higher at present.

1. INTRODUCTION

The estimation of rates of active crustal deformation over geological timescales is a topic with implications for seismic hazard assessment and for the understanding of related geodynamic phenomena. It presents challenges that require multi-disciplinary approaches involving e.g. geomorphology, stratigraphy, geochronology, Quaternary geology and structural geology (e.g. Keller and Pinter 1999; Burbank and Anderson 1999). Successful examples of multidisciplinary active-tectonic studies are abundant, but the ideal "ingredients" for such studies are often difficult to find in a given area of interest. Geomorphic or geological features that can serve as markers for the measurement of deformation rates may be very fragmentary and/or difficult to date (or, to date where needed the most). In areas where deformation rates are constant in space or, at least when a regular pattern of deformation is evidenced by the geometry of geomorphic or geological markers, deformation rates from given localities can be extrapolated to nearby areas of interest and, chronological constraints obtained in one location can provide cross-checking of dating results at another. These advantages are lost in areas of increased tectonic complexity, where datable markers may be necessary in very specific locations if meaningful estimates of broad-scale deformation rates are to be obtained and, chronologies established at one locality cannot be extrapolated to other localities due to uncertainties in the structural context. Non-constant deformation rates over time may further complicate matters. The case study herein is perhaps an example of most of the above problems. Nevertheless, even when all the above factors come into play, conservative interpretations of preliminary data may still provide useful constraints on deformation rates (minima / maxima) and guidance for the targeting of further studies.

This study refers to quantification of long-term coastal uplift rates, a classic topic of active tectonics studies (e.g. Lajoie *et al.* 1991; Ota *et al.* 1996). The interaction between coastal geomorphic/sedimentary processes and an uplifting fault block, can lead to the formation and preservation of a geomorphic and stratigraphic record of the uplift through time, consisting of uplifted marine terraces and associated marine deposits (e.g. Keller and Pinter 1999). Dating of such uplifted marine features provides estimates of the rate of coastal uplift. If any existing "regional" component of this uplift is removed, coastal uplift then becomes a measure of fault footwall uplift, which can be used to estimate fault slip rate (an important element for the assessment of the seismic hazard posed by the fault that causes the uplift). Such estimations can utilise fault dislocation models (e.g. Armijo *et al.* 1996; De Martini *et al.* 2004; Cianetti *et al.*, 2008) or, ratios between observed cumulative footwall uplift and hangingwall subsidence (e.g. McNeill and Collier 2004).

The westernmost part of the Corinth Gulf (CG) (west of Aigion in Figure 1b) lies in the part of the Corinth-Patras Rift system where present extension rates are highest (reaching 14-16 mm/yr – e.g. Avallone *et al.* 2004). Highly active coastal faults accommodate a significant part of this extension. The footwall blocks of these coastal faults are subjected to rapid uplift, the long term rates of which are not yet fully resolved. Whereas well-preserved flights of Pleistocene marine terraces have allowed robust quantification of coastal uplift rates at the eastern and central part of the North Peloponnesus coast (e.g. Dufaure and Zamanis 1980; Keraudren and Sorel 1987; Armijo *et al.* 1996; Leeder *et al.* 2003), moving towards the western extremity of the CG, terraces are generally scarce due to intense erosion, intensely faulted and/or difficult to date (McNeill and Collier 2004; De Martini *et al.* 2004; Trikolas *et al.* 2004, referring to the footwall blocks of the Eliki and Aigion faults; Efz and Af in Figure 1b).

Middle-Late Pleistocene uplift rates along the south coast of the Corinth Gulf (from Aigion westwards) and along the Rion Straits apparently increase towards Mount Profitis Elias (~745 m, PE in

Figure 1b; e.g. Kontopoulos and Zelilidis 1997; Sorel and Lemeille 2003; Palyvos *et al.* 2007 and references therein), where the highest remains of Middle-Late Pleistocene marine deposits occur (Doutsos and Poulimenos 1992). Conservative interpretations of available data in the Profitis Elias area suggest an uplift rate of 1.6-1.8 mm/yr minimum (time-averaged estimate since MIS11, and from uplifted Holocene shorelines; Palyvos *et al.* 2007, 2008). It is unknown just how much higher is the uplift rate in the fastest uplifting areas. West of Profitis Elias, published uplift rate estimates range from 0.4 to 4 mm/yr or more (Stamatopoulos *et al.* 1994, 2004; Houghton *et al.* 2003). The smallest values (Houghton *et al.* 2003; Stamatopoulos *et al.* 2004) refer to small fault blocks at the intersection of Pfz and RPfz, and are thus minima for uplift rate farther inland, whereas the highest values could reflect apparently younger ages from U-series dating of corals and molluscs in loose clastic deposits (Stamatopoulos *et al.* 1994/2004, Palyvos *et al.* 2007). In the area between Aigion and Profitis Elias, data on late Middle-Late Pleistocene uplift rates do not exist.

This paper regards the fragmentary record of late Middle – Late Pleistocene uplift (<400 ka) along a transect in the area between Aigion and Profitis Elias (Figure 1b). It discusses remnants of marine terraces and shallow marine sequences deposits, the results of dating attempts, and the constraints that we obtain on coastal uplift rate at different locations. We estimate the timing of the recent initiation of uplift, which was caused by migration or localization of fault activity on the presently active coastal fault zone (ANELfz; Figure 1b). The final goal being the provision of data that are useful for the estimation of the slip rate of this active coastal fault zone, we evaluate local uplift rate estimates in this respect, with reference to the morphotectonic context of differential uplift of secondary fault blocks and of possible increase of uplift rate with time.

2. ACTIVE TECTONIC CONTEXT

Currently, the most active part of the Corinth Rift coincides with the Corinth Gulf (CG) basin, which has a WNW-ESE trend and consists of roughly E-W-striking, predominantly N-dipping, right-stepping normal fault zones (Figure 1b/c) both on land (e.g. Doutsos and Poulimenos 1992; Roberts and Koukouvelas 1996; Goldsworthy and Jackson 2001; Zygouri *et al.* 2008) and below sea-level (e.g. Brooks and Ferentinos, 1984; Stefatos *et al.* 2002; Lykousis *et al.* 2007; Bell *et al.* 2008), which accommodate N-S extension (e.g. Sebrier 1977; Mercier *et al.* 1979; Briole *et al.* 2000). Active deformation is accompanied by intense seismicity, both historical (e.g. Ambraseys and Jackson 1997; Papadopoulos *et al.* 2000) and instrumental (e.g. Hatzfeld *et al.* 2000; Lyon-Caen *et al.* 2004).

At present, the westernmost part of the Corinth Rift is deforming the fastest, with geodetic extension rates reaching up to 14-16 mm/yr (e.g. Briole *et al.* 2000; Avallone *et al.* 2004; Bernard *et al.* 2006). In the area of interest, the main fault zones on land are the Lakka fault zone (Lkfz in Figure 1b; Poulimenos and Doutsos 1992; Flotté 2003) and the Aigion-Neos Erineos-Lambiri fault zone (ANELfz; Palyvos *et al.* 2005, 2007), which includes the "Kamares fault" (Bernard *et al.* 2006; "Selianitika fault" in Flotté 2003), and the Aigion fault (e.g. Koukouvelas and Doutsos 1996; Af in Figure 1b). The Pleistocene deposits that accumulated on the hangingwall of the Lkfz (Figure 1d) are found today uplifted up to 745 m above sea-level (at Mount Profitis Elias; PE in Figure 1). This indicates that the Lkfz is no longer active as in the past (e.g. Flotté 2003). The active or, most active fault zones today, are the coastal ANELfz (in the footwall of which part of the Pleistocene rift fill has been uplifted) and offshore faults to its North (e.g. Bell et al., 2008). This configuration is either the result of a basinward migration of faulting, i.e. abandonment of the Lkfz and development of the ANELfz on its hangingwall block (a process described elsewhere in the CG e.g. by Sorel 2000; Goldsworthy and Jackson 2001; Flotté *et al.* 2005) or, strain localisation on the ANELfz, following earlier stages when rift activity was distributed to both the Lkfz and the ANELfz (a process described farther east in the CG, at a broader scale, by Collier and Jones 2004).

3. EXISTING LITHO- AND CHRONO-STRATIGRAPHIC DATA

In the study area (Figure 2) the rift fill between the Lkfz and the ANELfz is dominated by lacustrine/fluviolacustrine and brackish deposits, with least one purely marine intercalation. These deposits were assigned an Early Pleistocene age in the earlier literature (Frydas 1989, in Poulimenos 1991). In the following, we refer to all of these deposits in Figure 2 as the "Synania formation" (Sf, an informal, polygenic lithostratigraphic unit). The Sf is predominantly fine-grained, containing intercalations of littoral sands and gravel. Poulimenos (1991) also reports large scale cross-beds (foresets) and slump folding in fine-grained lacustrine deposits "NE of the Aravonitsa area".

The Sf deposited in conditions of fluctuating salinity (Frydas 1989 in Poulimenos 1991; Frydas 1991), due to the existence of sills on both the W and E extremities of the Corinth and Patras Gulfs basins (e.g. Keraudren and Sorel 1987; Frydas 1991; Piper *et al.* 1990 and references therein). Since the late Middle-Late Pleistocene, sea level in the Patras and Corinth basins has been controlled by the Araxos and Rion

Sills (e.g. Piper *et al.* 1990a; Chronis *et al.* 1993; Perissoratis *et al.* 2000), and by the emergence of the Corinth Isthmus (Collier and Thompson 1991).

In the area of Mount Profitis Elias (PE), the rift fill is dominated by a formation of gravels (Figure 1d) ~600 m thick (Doutsos *et al.* 1988), which were deposited in alluvial fan and braided river environments (Kontopoulos and Zelilidis 1997). These gravels are considered of Pleistocene age (Symeonidis *et al.* 1987 in Frydas *et al.* 1995, Kontopoulos and Zelilidis 1997). Predominantly fine-grained lacustrine, brackish and marine deposits that are equivalent to the upper part of the Sf, overlie the alluvial gravel in the PE (Ano Zeria) area (Figure 1d). Frydas (1991) studied diatom assemblages within these Sf deposits, specifying that they are equivalent to biozone MNN20 (440-270 ka; Lourens *et al.* 2004 or, 467-265 ka; Raffi *et al.* 2006). He proposed an age estimate of "around 400ka", indicating that the Sf includes deposits younger than previously believed.

In the area of the Aravonitsa plateau (Figure 2), the Sf is overlain by a formation of gravel and sands (the Aravonitsa formation -Af-, an informal lithostratigraphic unit). The Af overlies unconformably the Sf (Poulimenos 1991), which dips here 18–30^{o} to the South (Figures 2a and 3a). Poulimenos (1991, 1993) mapped the Af as alluvial fan deposits, whereas Flotté (2003) mapped it as marine fan-delta deposits and attributed the emergence of the fan-delta to the shifting of fault activity from the Lkfz to the presently active coastal fault zone. Based on the chronology that Flotté (2003) proposed for the Aravonitsa plateau (MIS7, from extrapolation of uplift rates reported in neighbouring –but distant- areas, not direct dating), he placed this transition to ca. 200 ka BP.

Other previously recognised post-Sf deposits (not dated) include a gravel formation at Neos Erineos (Figure 2, considered to be alluvial fan deposits by Poulimenos 1991, 1993, and fan-delta deposits by Ghisetti and Vezzani 2004), and marine deposits related to terraces at Galatas and Andraousta (just SE of Figure 2, Flotté 2003; Ghisetti and Vezzani 2004; Trikolas *et al.* 2004).

4. STUDY METHODS

Geomorphological and geological observations for the detection of marine terrace remains and the determination of their morphotectonic context were carried out in the field, on aerial photographs of 1:15,000 / 1:30,000 scale and DEMs constructed from 1:5,000 and 1:50,000 maps of the Hellenic Army Geographical Service (HAGS). Inner edge elevations of mapped terrace remnants were derived from 1:5,000 HAGS topographic maps (contour interval: 4 m), and the associated errors are estimated to be of the order of 4-8 m (map error and error due to burial by colluvium). At key outcrops, stratigraphic logs were measured, analyzed *in situ* and interpreted, with particular attention paid to sedimentary, palaeontologic and palaeoenvironmental features. Extensive and repeated searches for material potentially suitable for U-series dating were conducted. Age estimates for marine deposits were obtained by: a) U-series dating of corals and synsedimentary carbonate crusts (hard grounds) retrieved from non-cemented clastic sediments (because no other, more suitable material could be found) and, b) calcareous nannoplankton analyses of fine-grained deposits.

Samples of fine marine deposits were examined by SEM (Jeol JSM 6360, University of Athens, Department of Historical Geology and Palaeontology) and light microscope for calcareous nannoplankton content following standard methodology (Thierstein *et al.* 1977; Perch-Nielsen 1985). U-series dating was conducted with the total sample dissolution method following the procedures in Bischoff and Fitzpatrick (1991), and the isotopic composition of samples was determined by alpha spectroscopy. The mineralogical composition of coral skeletons and crust samples was checked by X-ray diffraction prior to U-series analysis. Some coral specimens had traces of calcite and magnesian calcite, which clearly confirms contamination from weathering processes or from other organisms infilling the septa.

Nannoplaknton analyses were employed in order to have independent chronological constraints against which to compare U-series dating results, considering that the geological context of the analysed samples does not guarantee a chemically closed system (a basic prerequisite of the U-series method), and that none of the existing mineralogic, textural and isotopic criteria for evaluating possible open-system behaviour of the U-Th isotopes are self-consistent (e.g. Stirling *et al.* 1995), i.e., even after rigorous screening of coral samples prior to U-series analyses, erroneous ages can still be obtained even with high-precision dating methods such as TIMS (e.g. Dia *et al.* 1997). Even in apparently closed systems, with coral skeletons of pure aragonite, the incorporation of secondary aragonite can also occur (Lazar et al. 2004). In addition, alpha decay can result in the fragmentation of particles into smaller recoil nuclei which cause a selective migration of radioisotopes (Thompson et al. 2003). The above considerations, together with the scarce amount of coral available in some cases suggest that the U-series results obtained herein should be interpreted with extra caution.

5. THE ARAVONITSA PLATEAU AND THE ARAVONITSA FORMATION

The Aravonitsa plateau is a remnant of a flat depositional geomorphic surface at 500-520 m a.s.l. (Figure 2a). Most of the plateau surface is capped by a thick “terra rossa”, a soil that formed under warm and humid Mediterranean climate (e.g. Durn 2003). This soil typifies abandoned geomorphic surfaces in the broader area of the CG (typically, marine terraces underlain by littoral gravels rich in limestone clasts; e.g. Dufaure 1975; Keraudren and Sorel, 1987). The deposits of the Aravonitsa formation (Af) that underlie the Aravonitsa plateau, belong to different depositional environments and to several high-frequency depositional sequences or parts of sequences, internally partitioned by unconformities (sequence boundaries). As discussed in the following, they contain both alluvial fan (Poulimenos 1991) and fan delta deposits (Flotté 2003), as well as nearshore deposits.

5.1. Fan-delta and nearshore deposits

A large cliff at L1 (Location 1; Figure 2a) provides a characteristic view of the stratigraphy at the northern part of the Af (Figure 3b and c). The exposed strata at the uppermost part of the section were initially sub-horizontal, and now have an apparent dip of 171/06 (apparent dip direction/apparent dip), due to tilting. The tilting at L1 does not seem to have affected the whole plateau area. It appears to be local, related to a N-dipping fault (e.g. F2, or a non-visible fault along the valley ~250 m to its north).

At L1, the Af is subdivided into three facies successions (Walker 1990) or parasequences (Van Wagoner *et al.* 1990), labelled p1 to p3 in Figure 3b/c and 4a. The lower parasequence (p1) is about 21 m thick, and is composed of medium sized clinostratified gravels. These gravels are organised into parallel, concave up, large-scale cross-beds, truncated at their top by a planar erosive surface (gently-dipping to the N, before tilting). At the distal part of p1, the gravel cross-beds become finer down-dip and pass laterally to gentler dipping, planar layers of predominantly fine-grained deposits (area indicated with star in Figure 3b). These fine-grained deposits belong to the uppermost part of the Sf in our lithostratigraphic subdivision, but in a sequence-stratigraphic context, they belong to p1. Parasequence 1 is interpreted as a Gilbert-type fan delta, with the clinostratified gravels corresponding to delta front deposits (foresets) and the chronostratigraphically equivalent Sf fine-grained deposits to the lowermost part of foresets, to bottomsets and distal pro-delta deposits. Gilbert-type fan deltas occur commonly in both the uplifted ancient rift fill (e.g. Poulimenos *et al.* 1993; Dart *et al.* 1994; Malartre *et al.* 2004; Ford *et al.* 2007; Rohais *et al.* 2007) and the actively depositing one (e.g. Piper *et al.* 1990b). The foresets in p1 dip 17-22^{o} to the E or NE (Figure 2a), implying a fan delta depositional system that was fed by an ancestor of the Phoenix River (Figure 1b).

Parasequence (p2) is up to ~7 m thick and consists of cross-bedded, coarse sands, which interfinger upwards with clinostratified, prograding gravels (see small-scale foresets and topsets in Figure 3c). On the basis of recognised geometrical and sedimentological characters, p2 is interpreted as a coarsening-up, progradational, gravel beach sequence (*sensu* Massari and Parea 1988), developed in a coastal, wave dominated environment under microtidal regime and high rate of sediment supply. P2 is marked at the base by a transgressive surface, followed upward by shoreface sands laterally interfingering with clinostratified gravels. The oblique-sigmoidal pattern of clinostratification (Figure 3c) is a typical feature of the gravel beachface sub-environment, with foresets corresponding to high relief ramps of the lower beachface (or plunge steps) and topsets to the upper beachface and foreshore (Massari and Parea 1988; Bardaji *et al.* 1990). Parasequence 2 is also interpreted as a single small-scale regressive *R cycle* (Zecchin 2007), with the transgressive phase represented by the basal bounding surface. The offlap break between foresets and topsets precisely marks the ancient base level position. Parasequence 3 (p3) is up to 10 m thick and consists of coarse sands, with a few gravel intercalations mostly close to the base, arranged in planar, initially horizontal beds that are attributed to the shoreface environment.

Parasequence 3 is considered to be marine, on the basis of palaeontologic content: very rare specimens of *Ostrea* sp. were found at L2 on the ploughed surface of a vineyard, and rich marine nannoflora is present in a fine-grained intercalation at L3, where the base of p3 is exposed in an accessible outcrop (where no marine macrofauna or ichnofossils were found). Robust evidence of the depositional environment of the p1 gravel foresets is lacking. Flotté (2003) mentions marine macrofauna in them, but he does not give further details. In all accessible foreset outcrops, we could not find any trace of marine macrofossils or ichnofossils. Absence

of such evidence of course, does not necessarily suggest that the p1 fan-delta was not marine. More robust evidence comes though from fine-grained p1 deposits, exposed on roadcuts at L5. These deposits comprise a light brown/beige package, which caps whiter-coloured fine-grained lacustrine deposits. The colour contrast, as well as down-stepping of the respective contact caused by small faults are best discernible in distant views, looking from the East. Within the p1 package, large-scale cross bedding as well as slump folding are observed (Figure 4b). Poulimenos (1991) presumably refers to L5 when he reports such features "in lacustrine deposits NE of Aravonitsa". The clinostratified fine-grained p1 deposits at L5 are interpreted as the lowermost part of fine-grained p1 foresets. Their dip is 005/35, whereas gentler-dipping pro-delta deposits below them, dip ~20^{o} to the N/NNE. Initial dips were smaller (the package is tilted to the North). The northerly dip direction of the p1 fine-grained foresets at L5 is consistent with the direction of p1 gravel foresets immediately to the SW of L5. The L5 foresets contain occasional "floating" large pebbles and at least one gravel layer, features identified also by Malartre *et al.* (2004) and Ford *et al.* (2007) in fine-grained bottomset-prodelta deposits of the uplifted Gilbert delta of the Vouraikos River further East (Figure 1d). The fine-grained foresets at L5 contain the lacustrine bivalve *Dreissena polymorpha,* indicating that the p1 fan delta prograded during a period when the CG was a lake, i.e. during a period when eustatic sea-level was lower than the elevation of the sill at the time (i.e., not only during a eustatic sea-level low-stand). Brackish fauna (*Mytilus* sp.) was found within the pro-delta deposits underlying the foresets at L5 (Figure 4b).

5.2. Sequence stratigraphic interpretation

In the following, we discuss the Af deposits in a sequence-stratigraphic context (e.g. Van Wagoner *et al.* 1990; Emery and Myers 1996), with reference to relative base level (RBL) changes. RBL changes reflect both base level (BL) changes and vertical tectonic movements. Past BLs in the sill-controlled CG have corresponded to either sea or lake level. The scenario given below is based on the assumption that BL changes were the dominant control on RBL change, causing RBL changes that were much faster than those caused by vertical tectonic movements. This assumption is not arbitrary, since the discussed deposits accumulated during the transition from a regime of tectonic subsidence to one of uplift, i.e. when vertical tectonic movements were expectedly relatively mild (see discussion section).

Fan delta progradation during the deposition of p1 indicates that sedimentation rate outpaced the rate of creation of accommodation space, which is in our scenario is predominantly controlled by the rate of RBL change. The simplest possible interpretation is that this happened during a RBL still-stand that corresponds to a base level still-stand (lake level still-stand in this case, because p1 is lacustrine). Consequently, the p1 gravels are interpreted as regressive and are attributed to a lacustrine Highstand Systems Tract (HST) (Figure 4a). The upper part of the p1 foresets is truncated by an initially N-dipping erosive surface. This erosive surface is interpreted as a Sequence Boundary (SB1, separating sequences S1 and S2; Figure 3b). Erosion of p1 complies with a RBL fall (lake level fall, or tectonic uplift). Whether topset strata existed in p1, is unknown because of erosion.

The "lacustrine highstand" mentioned above, should not be confused with "eustatic sea-level highstand". This lacustrine highstand took place when eustatic sea-level was lower than the lowest-lying sill that was controlling the communication of the CG with the open sea at the time. Non coincidence between fluctuations of lake and sea levels (i.e., their being out of phase) is a common feature in the Mediterranean area. This is due to the different effects of the dominant controlling factors and related interplays (such as climate and tectonics for lake basins vs. eustacy for marine basins), on sedimentation and local base levels (Leeder *et al.* 1998). Thus lacustrine HSTs may develop at the same time as eustatic sea-level is falling, low-standing or rising, for as long eustatic sea-level remains lower than the lowest-lying sill that controls the communication of the CG with the open sea in a given period.

Parasequences 2 and 3 belong to a younger marine sequence (S2). The basal bounding surface of parasequence 2 is interpreted as a trangressive surface (TS) that is superimposed on and coincident with sequence boundary SB1. The clinostratified gravels of p2 indicate progradation, i.e. that sedimentation rate outpaced the rate of RBL change, the simplest interpretation being that this happened during a BL stillstand. Judging from the thickness and fining up trend of facies within p3, we infer that p3 was deposited under a phase of RBL rise, arguably caused by BL rise. BL rise corresponded to eustatic sea-level rise, since marine micro and macro fauna in p3 indicate that the sill was overtopped by sea-level at the time. The surface between p2 and p3 is interpreted as a flooding surface. At L1, p3 is composed of deeper shoreface sands; beachface deposits are lacking. Farther SW, at the more landward L2, nearshore deposits occur at a higher stratigraphic position, suggesting a retrogradational facies pattern for p3. The general stacking pattern of p2 and p3 together, from shoreface/beachface (p2) to shoreface (p3 at L1) and nearshore deposits (p3 at L2), is also retrogradational, p2 corresponding to an episode of progradation during a short-lived BL still-stand superimposed on a general trend of BL (eustatic sea-level) rise. We thus attribute p2 and p3 to the Transgressive and probably to the Highstand Systems Tracts (repectively) of the upper, marine sequence in the Af (Figure 4a). In this interpretation, p3 records the highest-reaching marine transgression in the area of Aravonitsa.

5.3. Parasequence 3 as a past sea-level highstand marker

The highest-reaching part of p3 can be used a sea-level highstand marker (a depositional terrace), accepting that the Aravonitsa plateau and p3 have not been subjected to more than a few metres of denudation (as the plateau morphology seems to suggest). A pronounced scarp -trending NNW-SSE- that traverses the plateau immediately to the NE of the Aravonitsa village, could be the remnant of a palaeo-coastal cliff, i.e. an erosional feature coeval to the sea-level highstand the p3 deposits correspond to. However, it could also be the geomorphic expression of a fault (F1 in Figure 2a). E.g., Poulimenos (1993, 2000) does trace here a fault with similar direction. Faulting has most probably affected the plateau at L2 (F2), as suggested by a gentle scarp on which p3 deposits outcrop at the surface (terra rossa has been eroded away). Flotté (2003) includes F2 in a longer structure extending farther NW (we consider it a small, local fault instead).

If F1 is presumed to be a fault, p3 marine deposits would be preferentially preserved on its downthrown block, and conversely, p3 deposits on the upthrown block may have been eroded away. If our map trace of the Af/Sf limit is correct, possible throw on "F1" on either side of the plateau was less than 10 m, if not inexistent. The height of the "F1" scarp on the plateau may be the result also of erosion (along a possible small fault, i.e. a fault-line scarp), as suggested by the presence of a small erosional depression in front of it (containing Holocene deposits - Figure 2a). Given the high elevation of the plateau (500-520 m a.s.l.), if limited denudation and potential throw on F1 introduce an error even of 20-30 metres in the determination of the p3 highstand shoreline, this error would nevertheless be small in percentage terms.

5.4. Alluvial fan deposits

Alluvial fan deposits were recognised in the area of L25 (Figure 2a), overlying the fan delta gravel of p1. These alluvial fan deposits are the youngest stratigraphic unit (sequence) in the Af. In the proximal part of the Aravonitsa formation alluvial fan deposits presumably belonging to the same sequence (S1) as the fan delta gravel, are exposed on a roadcut at L27. In Figure 2a, grey colour is used for areas where alluvial fan/fan delta deposits were not discriminated.

5.5. The Aravonitsa unconformity

The lower part of the Sf deposits below the Af in general, and at L8 and L9 in specific (i.e., very close to L1), are strongly tilted (17-30^{o}) towards the south (Figures 2a and 3a). In contrast, the Sf deposits at L1 have a sub-horizontal apparent dip in a N-S direction (Figure 3b, the cliff trends N-S). The exposure is not enough to identify the relationship between these Sf deposits and the deeper, strongly tilted Sf deposits (exposed at L8). In at least one nearby location though, on a large NNW-SSE oriented cliff at L4 (Figure 6), an angular unconformity between the two is discernible (the "Aravonitsa unconformity" - AU). The true dip of the deposits below the AU (the lower Sf or "lSf") is estimated at 193/24 (dip direction/dip) based on apparent dip measurements on the cliff at L4 and nearby ones. This estimate agrees with a large number of true dip measurements at accessible outcrops in the surrounding area (Figure 2a). In contrast, the Sf deposits above the AU (the upper Sf or "uSf") have an apparent dip of 345/01-02 (direct measurement or estimate of their true dip was not possible).

Apart from L4, an angular unconformity within the Sf can be discerned also on the cliff at L8. In the cliffs between L5 and L6, an angular unconformity between uSf deposits (fine-grained foresets and underlying brackish and lacustrine strata) and lSf deposits was not identified. In the broader area of L5, L6 and L28, both the uSf and lSf deposits have the same northerly dip direction, varying locally due to small faults and minor warping. The change from southerly lSf dips all over the broader Aravonitsa plateau area, to northerly in the area of L5, L6 and L28, seems to be abrupt (Figure 2a). This indicates that the latter area belongs to a different secondary fault

block within the broader hangingwall block of the Lkfz, highlighting the structural complexity of this area. In this context, an angular unconformity like that in L4 may not exist in the area of L5, L6 and L28, or, it may be much less pronounced and difficult to discern, considering also the orientation of cliff outcrops and the available viewpoints.

5.6. Marine deposits at the periphery of the Aravonitsa plateau

Near the western side of the Aravonitsa plateau, at L10 in Figure 2a, a very well-defined marine layer occurs within strongly (30^o) south-tilted lacustrine deposits of the lower Sf (see also Figure 5). The relevant outcrop exposes a deepening-upwards succession with littoral sands at the base giving way to nearshore silts and sands with a very rich marine macrofauna assemblage including *Cladocora caespitosa* corals (details in Figure 7a). The assemblage is typical of temperate-warm, shallow sea and of mixed carbonate-terrigenous, infralittoral environment (Peirano et al. 2004, and references therein). The nearshore marine deposits are ~2.5 m thick and change quickly to sands and silts with abundant brackish-water macrofauna, followed by marls with purely lacustrine macrofauna. The palaeoenvironmental change recorded in a few metres (~4 m), from purely marine to brackish and then to lacustrine environment, without any intervening unconformity, can be attributed to the salinity fluctuations in the CG driven by eustatic sea-level fluctuations, as proposed by Frydas (1991) on the basis of micropalaeontological studies in neighbouring occurrences of the Sf. From a stratigraphic standpoint, the marine layer at L10 is the oldest layer with clearly marine macrofauna that we could find within the lSf in the study area.

Around the Aravonitsa plateau, marine or brackish macrofauna is found at several other locations (squares in Figure 2), either reworked in colluvial deposits or *in situ* in outcrops. At L7 (372 m a.s.l.), marine macrofauna includes very rare *Cladocora caespitosa* pieces. This fauna was found in colluvium in front of small landslide scars just below the interfluve; therefore, it is not known if it originates from sediments within the Sf or from a younger marine sequence (now eroded away). Brackish (and marine?) macrofauna within the Sf, was found also at L8 and L9.

Very rich marine macrofauna is found at L11 on a scraped field surface, in strata with apparent dip to the SE (Figure 8a). The large variety of species (details in Figure 4c) includes *Flabellum* sp. corals (very rare, found only after the fourth visit to the site, after heavy rains; Figure 8d). The fossiliferous layer is correlated with fine-grained deposits ~1.5 m thick with marine macrofauna that crop out at a roadcut 30 m to the NE (Figure 8b, Figure 4c). The entire marine package (a small depositional sequence) overlies with angular unconformity strongly SSE-tilted (32^o) lacustrine Sf deposits (just outside Figure 8b, to the right) and it is covered by very coarse gravels, which correlate with alluvial fan deposits that outcrop further west along the road to Aravonitsa (unit 6 in Figure 2a).

The stratigraphic relationship of the marine layer at L11 with other marine deposits in the broader Aravonitsa area (p2 and p3 within the Af, or the marine layer at L10 within the lSf) is not apparent, due to lack of adequate exposures. The very rich macrofauna at L11 is similar to that at L10, but, the angular unconformity between the marine deposits at L11 and the underlying Sf deposits, as well as the lack

of gradual upwards transition to lacustrine deposits (observed at L10), suggest that the marine deposits at L11 may belong to a younger sequence. It is only micropalaeontological analysis (next section) that verifies this definitively though.

6. Chronological constraints on the marine deposits in the broader Aravonitsa area and uplift rate estimates

6.1. Chronological constraints on marine deposits

Because the water level and salinity of the CG has been sill-controlled since at least MIS11, marine conditions in the Gulf may be expected during, and close in time to eustatic sea-level highstands, when the controlling sill was overtopped by rising sea-level. This context is a favourable factor for the establishment of the chronology of the marine deposits not associated to marine terraces, because these deposits are expected to date close to sea-level highstands. We note that, if the controlling sill had a general shallowing trend moving back in time, only the highest-reaching highstands will be present in the stratigraphic and geomorphic (terrace) record as one moves back in time.

Nannoplankton analysis of silts within the nearshore sands of p3 at L3 identified biozone MNN20 (440-270 ka; Lourens *et al.* 2004 or, 467-265 ka; Raffi *et al.* 2006). Nannoplankton analysis of the oldest layer with purely marine macrofauna that is known within the lower Sf (L10), also identified biozone MNN20. Biozone MNN20 encompasses the MIS11 and MIS9 eustatic sea-level highstands. U-series dating of four samples of *Cladocora sp.* corals from L10 provided anomalously young ages of 160 - 200 ka (Table 1). Yet, given the stratigraphic context, they clearly contradict the micropalaeontological results at both L10 and L3. U-series dating of corals from clastic deposits (as opposed to corals from carbonate reefs, where a chemically closed system is more certain) can be problematic (e.g. Dia *et al.* 1997). X-ray diffraction analyses of samples 4507 and 4607 show the occurrence of calcite and high magnesian calcite in the corals demonstrating diagenetic processes. Thus we conclude that the U-series ages at L10 refer to a diagenetic episode, rather than to the time of coral growth. Perhaps interestingly, similar ~160-170 ka ages (MIS6e, a small highstand during a glacial stage) have been recurring in areas to the West of Profitis Elias (Houghton et al. 2003; Stamatopoulos et al. 2004; Palyvos et al. 2007 and unpublished 3HAZ project data).

The lacustrine deposits between p3 and the marine layer at L10 deposited when sea-level was lower than the elevation of the sill that controlled the communication of the CG with the open sea at the time. These lacustrine deposits include a fan-delta sequence (p1) that corresponds to a considerable amount of time, judging from the amount of fan delta progradation involved. Given this stratigraphic context (Figure 5), the most likely (or, the only plausible) interpretation of the available data is that the marine layer in the lower Sf belongs to the MIS11 highstand (or, a MIS11 highstand if there were more than one) and p3, which corresponds to the

oldest marine “terrace”, to one of the MIS9 highstands, arguably the oldest of the two (MIS9c).

The stratigraphic context of the marine layer at L10 presents striking similarity with that of the oldest known layer with purely marine macrofauna inside the Sf in the nearby area of Ano Zeria (in Profitis Elias area, Figure 1d, outcrop described in Figure 7b). Both marine layers pass gradually to lacustrine deposits, without any intervening unconformity. The marine layer within the Sf at Ano Zeria has an age bracketed between 440-350 ka, based on micropalaeontological determinations by Frydas (1991), who reports diatom assemblages equivalent to nannofossil biozone MNN20 and gives an age estimate of “around 400ka”, and on U-series ages >350 ka obtained from *Cladocora* sp. corals in a correlative marine layer by Sorel *et al.* (2005, location described in Figure 7c). The only highstand included in this age range is that of MIS11 (around 400 ka). Based on these data, the correlation of the L10 marine layer to MIS11 is supported even further.

In the proposed interpretation, the lacustrine fan-delta parasequence (p1) can only correlate to MIS10. More specifically, to a period that corresponds with the MIS10 eustatic sea-level lowstand and to larger or smaller neighbouring parts of the eustatic sea-level curve that lie below the (unknown) elevation of the CG sill at the time. Based on the present-day elevation of the sill at Rion (Perissoratis et al., 2000), this period would correspond to ca. 40 kyr (according to the curves of Cutler *et al.* 2003 and Siddal *et al.* 2003 in Figure 9), and more, if a higher sill during MIS11-10 is assumed. Considering the above, the Aravonitsa unconformity dates within the early part of MIS10, i.e. sometime between ~390 and ~350 ka BP. Older ages in this range are preferable, to allow more time for progradation of the fan delta in p1.

Micropalaeontological analyses of calcareous nannoplankton in two samples from the fine-grained shallow marine deposits at L11 (Figure 8b) yielded nannoplankton assemblages in highly diluted terrigenous material, with rare specimens (approx. 1%) of *Emiliania huxleyi* (Figure 8c) in countings of ca. 300 placoliths, enabling the biostratigraphic correlation with MNN21a biozone. According to the astronomically tuned biozone timescale of Lourens *et al.* (2004), the base of the MNN21a, which is defined by the lowest occurrence (LO) of *Emiliania huxleyi*, is at 270 ka in the eastern Mediterranean (265 ka, according to Raffi *et al.* 2006). Based on four sea-level curves in Figure 9, the LO of *Emiliania huxleyi* in the stratigraphic record of the eastern Mediterranean falls within a period of low sea-levels. During this period, the Corinth Gulf was expectedly a lake, isolated from the sea by a sill. Depending on the elevation of the sill at the time, the LO of *Emiliania huxleyi* in the CG is thus expected more or less close to the MIS7e highstand (i.e. a few kyr before 240 ka), because only then sea-water with *Emiliania huxleyi* had the chance to enter the CG. This places the marine deposits at L11 at the MIS7e or a younger highstand. In all probability the MIS7e, otherwise *Emiliania huxleyi* must have been more abundant (although, the neritic character of the studied material should always be taken into account). Considering the above, and also that the stratigraphic configuration at L11 suggests an age close to a highstand of relative sea-level (arguably, corresponding to a highstand of eustatic sea-level), we consider that the likeliest age of the marine deposits at L11 is ~240 ka.

U-series dating on corals from L11 (*Flabellum* sp.; Figure 8d) gave an age of 283.621 +40.040/-29.558 ka (Table 1). The minimum possible U-series age (~254 ka) is safely older than the *local* LO of Emiliania huxleyi that is predicted in the context of sill-controlled communication of the CG with the open sea. Based on this context,

we infer that the U-series age is in all likelihood an apparently older age, or, that the dated corals have been reworked from pre-MIS7e marine deposits.

6.2. Uplift rate estimates

As discussed earlier, the highest-reaching part of p3 under the Aravonitsa plateau (500-520 m) can be taken as a proxy for a past sea-level highstand. Based on the chronology established in the previous section, this highstand can either be MIS9c (preferred) or MIS9a. If we assign p3 to the MIS9c highstand, we obtain average uplift rates (AURs) of 1.47-1.61 mm/yr (using the four curves in Figure 9). If we assign p3 to the MIS9a, we obtain higher AUR estimates of 1.67-1.87 mm/yr. These values are minima (expectedly close to true values), due to erosion of p3. We prefer correlation of p3 to the MIS9c highstand, because if p3 correlates to MIS9a, we need to accept that all of sequence S2 (Figure 4a) belongs to MIS9a, and that all of the MIS9c sequence has been eroded. With the MIS9c highstand at 500-520 m, the MIS9a highstand terrace would be expected at 440-460 m a.s.l. The fact that we cannot recognise remains of a marine terrace or depositional sequence at these elevations means little, given the very intense erosion all around the Aravonitsa plateau.

Assigning L11 to MIS7e, translates to an AUR of 1.71-1.85 mm/yr (Figure 9), or slightly higher, to allow for displacement by faults and uncertainty about the exact highstand shoreline position. Displacements on exposed faults are small, of the order of 1-2 m (one of the faults shows in Figure 8b), but this could be misleading. The highstand shoreline could well be at L11 though, considering the stratigraphic configuration at L11 (Figure 4c).

With the uplift rate we obtain at L11, there is a good correlation of p3 to the MIS9a highstand (allowing for some erosion of p3 and thus, somewhat higher highstand elevation). This correlation we do not favour, as mentioned previously. The apparent controversy stems from the assumption of constant uplift rate between MIS9 and MIS7e. This assumption is not at all necessarily valid in our area. On the contrary, uplift rate can be reasonably expected to increase with time, especially between MIS9 and MIS7e, a period close to the initiation of uplift (see discussion).

7. THE SELIANITIKA TRANSECT

7.1. Marine deposits and terrace remnants

At the Selianitika transect, the highest remnant of marine deposits are cemented conglomerates with very rare fragments of marine bivalves that occur at 348 m a.s.l. (Figure 2b). These conglomerates are discordant above tilted Sf deposits and are interpreted as transgressive littoral (beach) deposits. A fault (F3) downthrows the gravel by a few metres, whereas it has accommodated a larger throw in the

underlying Sf deposits. Farther NW, the interfluve steps down abruptly by ~60 m. This down-stepping coincides with the NW tip of a continuous and straight, NW-SE trending, N-dipping fault that Koukouvelas and Doutsos (1996) mapped as the western part of the Aigion fault (their trace is shown with thick, pink coloured line in Figure 1d). In Figure 2b, we include two possible fault traces in this area (collectively labelled FZ2), which are based though on morphological indications only. Constraints on the cumulative throw on FZ2 are not available. The down-stepping of the interfluve could correspond –in part at least- to a paleo- coastal cliff formed during a sea-level highstand by marine erosion (modification by non-marine erosion also not being excluded). Erosion is indeed suggested by the absence of the 348 m conglomerates on the hangingwall block of FZ2.

Along profile A (the Selianitika transect *sensu stricto*), coastal terrace remnants -CTRs- are found at six levels to the NE of FZ2. Their inner edges lie at ~260, ~248, ~218, ~156, 124/112 and 76-80 m a.s.l. A well-defined CTR occurs also at 116-120 m in the area of L30. It is certain that at least some CTR or bench inner edges correspond to faults rather than highstand shoreline angles. Faults were observed in outcrops (red squares in Figure 2b; Figure 10c; Figure 11a) e.g. at the inner edges of the 152-156, 124, and 112 m CTRs or benches. In all cases, only minimum fault throws can be estimated. Faulting is very likely along the 116-120 m CTR inner edge and, possible also along the 218 m CTR inner edge and between the 260/248 CTRs. Due to faulting, the number of CTRs can be larger than the true number of initial coastal terraces (in all probability, it is). Along profile A and the neighbouring interfluve to the SE, more or less well-defined benches of unknown origin occur at various elevations a.s.l. (indicated with purple outlines in Figure 2b).

The CTRs at 260/248, 218 and 116-120 m consist of cemented gravel with terra rossa on top. One *Ostrea* sp. piece was found in the 248 m CTR slope wash. The 218 m CTR corresponds to a small fan-delta, with well-preserved foresets and topsets (Figure 10b). Large and thick *Ostrea* sp. shells are found within the topset gravels and, also in the slope wash deposits derived from them. Below the gravel foresets, in marine nearshore sands and silts exposed in a freshly ploughed slope at L32, we found recrystallised *Cladocora* sp. and *Spondylus* sp. The size and thickness of the *Ostrea* shells in the topsets of this fan-delta, together with the presence of *Spondylus* sp. in the nearshore deposits below the foresets (*Spondylus* sp. has been found only here), suggest the relatively warmest water conditions among all of the marine deposits in the study area, and make the 218 m fan-delta a possible candidate for the MIS5e terrace.

The CTR at 152-156 m is capped by a thin veneer of East-prograding foreshore gravel with *Lithophaga* perforations, that overlies a thick marine sequence of transgressive shoreface and beachface sands (“sequence A”; Figure 10c and 12a). The term “sequence” is used informally here and in the following. Sequence A can be followed in roadcuts down to ca. 84 m a.s.l., close to the elevation of the inner edge of the lowest CTR (~76-80 m a.s.l.). The marine nature of sequence A is testified by relatively rare *Pecten jacobaeus* at an outcrop at about 88 m a.s.l. and rare *Ostrea edulis, Anomia ephippium, Chlamys proteus* and *Patella* sp. at L31 (Figure 10c). The nature of the contact between the transgressive sands of sequence A and the thin veneer of the overlaying regressive gravels is not known, since we have not been able to observe this contact in outcrop, I.e. we do not know whether the gravels represent the topmost layer of a depositional terrace (hypothesis 1) or, whether they cover an erosional terrace, i.e. a shore platform cut onto the soft sands of sequence A

(hypothesis 2). In hypothesis 1, the gravel/sands contact would correspond to a boundary between two vertically continuous facies, in hypothesis 2 to an erosional unconformity or paraconformity. Which of the two hypotheses is the case for the 152-156 m CTR, is very important with respect to the interpretation of U-series dating results discussed in the next section. Hypothesis 2 is not at all unlikely, considering the soft lithologies at Selianitika (Sf and sequence A), which favour the formation of erosional coastal terraces. The 76-80 m and 116-120 m CTRs (next paragraph) are in fact erosional. Also the two prominent, large benches at 168 and 124 m on the interfluve SE of profile A, in all probability correspond to erosional CTRs.

The regressive marine gravel on the 116-120 m CTR rest on strongly back-tilted Sf deposits (Figure 2b) indicating an erosional CTR. This CTR correlates with the 124 m bench immediately to its NW, the elevation difference reflecting SE-tilting of the fault block these surfaces rest on (tilting is best discernible in distant views from Selianitika village on the coastal plain). The lowermost CTR is also erosional, cutting across strongly tilted Sf deposits. Two extensive CTRs belonging to the same erosional terrace occur SE of profile A, with inner edges at the same level (~76-80 m, with some variation) for a distance of about 850 m (Figure 2b). The persistence of the same inner edge elevation along this distance, suggests that the 76-80 m CTR inner edges in all probability correspond to a paleo-shoreline angle (buried by colluvium). Cemented marine gravels occur at 80-84 m a.s.l. on both sides of the valley at L30. On the northern side, these gravels seemingly continue under the marine sands below the 116-120 bench and we thus consider them as transgressive, and irrelevant to the 76-80 m coastal terrace. This may not be necessarily true on the southern side though.

7.2. Chronological constraints and uplift rate estimates

Inside the transgressive sands of sequence A just below the 152-156 m CTR, at an outcrop at L31 that is being subjected to progressive destruction by sand mining since at least 2003, syn-sedimentary $CaCO_3$ crusts up to ~1.5 cm thick were found (Figure 12a and b). As determined by X-ray diffraction, the crusts consist of pure calcite. Ichnological evidence, namely sponge and bivalve borings and worm tracks, as well as vermetid tubes and an *Ostrea* sp. shell that were found stuck on the crusts (Figure 12b to d), indicate that their formation was syn-sedimentary, i.e. that they formed before the deposition of the sand layers that lie immediately above them. Prismatic crystalline structure perpendicular to the crust microlaminae, with elongate crystals extending across microlaminae (Figure 12e and f), indicates recrystallisation (during diagenesis). In small-magnification (15X) visual examination, bio-erosional traces seem to cut the calcite crystals also, suggesting that recrystallisation preceded bio-erosion, i.e. that recrystallisation occurred shortly after the initial formation of the crusts.

Two samples of crust were analysed. The TS606 age in Table 1 does not result from full analysis (extended counts), due to electricity power failure at 2000 minutes, and is thus not discussed in the following. The fully analysed sample gave an age of 127.5 +6.4/-6.1 ka (TS1006 in Table 1) according to which, the dated deposits correlate to MIS5e. Cross-checking of the TS1006 U-series age by independent dating evidence is not available and, we cannot use the goodness (or non-goodness) of the correlation between successive marine terraces and peaks in the sea-level curve that results from the AUR derived from this age as a means to independently validate (or invalidate) it. This is so because the CTR staircase at Selianitika has been affected by

faults with appreciable throws. Throws are unconstrained, and thus no specific restoration can be given with certainty. Based on the negligible amount of contamination by ^{232}Th (Table 1), we consider that the TS1006 U-series age can be considered as a fairly safe indication of a MIS5 age though (especially if we consider also the TS606 age, even though it does not result from full analysis). Uncertainty remains however as to whether the stand-alone TS1006 U-series age can be taken as a safe indication of a MIS5e age.

Average uplift rate (AUR) estimation depends on (a) whether the 152-156 m CTR is depositional or erosional (hypothesis 1 or 2), (b) the exact age of the crusts (not known), and (c) further considerations discussed in the following. In hypothesis 1, the crust age is practically the age of the depositional terrace (shoreface sands of L31 and the gravel veneer together). In hypothesis 2, it is a maximum-limiting age for the erosional terrace and regressive gravels.

AUR-wise, the most conservative interpretation of the field observations ("scenario 1") stems from hypothesis 1 (a depositional 152-156 m CTR) and by taking the TS1006 age literally (MIS5e). This way, we obtain AURs of 1.11-1.21 mm/yr using different sea-level curves. Because the CTR inner edge does not correspond to a highstand shoreline angle (since it is fault-controlled), the above AUR is a minimum for the 152-156 CTR area, arguably, a minimum that is reasonably close to the true AUR in this specific area. Because of throw on fault 7, the AUR at the 152-156 m CTR area is in any case a minimum for the areas on the footwall block of fault 7.

A controversial point about scenario 1 is that it obliges us to correlate the fan-delta at 218 m to MIS7a (or, less likely, to an older highstand). Yet, the 218 m fan-delta topsets and the sands below the fan-delta at L32, contain the relatively warmest fauna found in all the study area, a fact that suggests possible correlation to the MIS5e highstand, although it does not definitively prove it. Such a correlation translates to 1.66-1.79 mm/yr minimum AUR for the area of the 218 m CTR. Minimum AUR, because the elevation of the highstand shoreline angle may not be at the 218 m CTR inner edge, due to faulting. This AUR estimate is not at all unrealistic, given: (a) the results at the Aravonitsa plateau, L11 and Neos Erineos (next section) and, (b) that throw on FZ2 (the western termination of the Aigion fault according to Koukouvelas and Doutsos, 1996) is unknown and could well be small during the last 125 kyr. In the above scenario, the CTRs at 248/260 m, could either be separate MIS6e terraces, the same MIS6e terrace disturbed by faulting, or even parts of the MIS5e terrace. In the latter case, AUR at the 260 m CTR would be around 2.0-2.1 mm/yr.

There are two ways to reconcile all available observations with a MIS5e fan-delta at 218 m. One way is to accept a depositional 152-156 m CTR belonging to MIS5c, in which case the TS1006 age is an apparently older age due to diagenesis ("scenario 2a"). A second way ("scenario 2b") is to consider (a) that the 152-156 m CTR is a remnant of an erosional marine terrace cut onto sequence A (hypothesis 2) and, (b) the dated sands of sequence A and those below the 218 m fan delta at L32 (informal "sequence B"), belong to *the same*, faulted sequence ("sequence AB"). In scenario 2b, the TS1006 age can be taken literally, since in three out of five sea-level curves, it includes the MIS5e highstand only marginally (Figure 9). I.e., it complies better with the hypothesis that the L31 sands correspond to an early part of the MIS5e transgressive sequence AB (as scenario 2 suggests), rather than with scenario 1, where we need to assume that the L31 sands belong to the MIS5e highstand.

Scenario 2b is possible structurally, considering the minimum vertical displacement of the base of fluvial unit 4d (Figure 11a) on fault 7. It also complies

with the constraints that the existence of a sill poses on the elevation difference between the MIS5e highstand shoreline and the lowest occurrence of marine deposits in sequence AB. Based on the present-day sill depth (-62 m), and considering +5 m of highstand elevation during MIS5e, this limit is about 67 m. This constraint is easily met with realistic (minimum) throws on faults 7, 5 and 2, as shown in the –crude-cross-section restoration in Figure 11b. This restoration does not take into account syn-sedimentary faulting during the deposition of sequence AB, which would allow for more than 67 m of elevation difference between the highstand shoreline and the lowest occurrence of sequence AB in the restored section. In the restoration scenario in Figure 11b, the highstand shoreline angle of the erosional terrace that the down-thrown 152-156 m CTR corresponds to, is placed at the inner edge of the 180-184 m bench on the footwall block of fault 7. This bench does not necessarily correspond to a coastal terrace though, it could be merely due to the lithological change from cemented fan delta gravel to the softer deposits in front of them. An alternative location is the inner edge of a less well-defined bench (more of a knick point on the interfluve) at 168 m. Considering that a well-developed bench occurs at 168 m on the interfluve SE of L32, this may be a more likely elevation for the original highstand shoreline of the 152-156 m CTR (before this CTR was downthrown by fault 7). In fact, with uplift rate obtained by assigning the 218 m fan-delta to the MIS5e highstand, the MIS5c shoreline on the footwall block of fault 7 would be at about 168 m (based on most curves in Figure 9). Figure 11c depicts a restoration scenario with the 152-156 m CTR restored to a 168 m highstand shoreline. In this case, fault 7 needs to be allowed syn-sedimentary slip during the deposition of sequence AB. Alternatively, a non-exposed fault between faults 6 and 7, which does not affect the 152-156 m CTR but only sequence A below it, can account for the remanent vertical displacement in the restored section.

The uncertainties in all the above, do not allow for a robust conclusion. Namely, there is uncertainty in the U-series ages, uncertainty about the nature of the 152-156 m CTR (erosional vs depositional), lack of fauna suitable for U-series dating at the 218 m fan delta, lack of enough data on fault displacements, and, the fact that the hypothesis that sequences A and B are parts of the same “sequence AB” cannot be proved or disproved due to erosion and non-exposure of “sequence AB” on the footwall of fault 7. In the final discussion of AUR estimates, we include both the most conservative interpretation (most conservative only AUR-wise; scenario 1) and the AUR estimate that results from correlation of the 218 m fan-delta to MIS5e (scenarios 2a/b).

8. THE NEOS ERINEOS TRANSECT

8.1. Marine deposits and terrace remnants

Along the Neos Erineos transect, the highest remains of marine deposits NE of L7 are shallow marine silts and sands with bivalve and gastropod macrofauna at L22 (290 up to ~302 m a.s.l.; Figure 2b). About 250 m to the NE of L22, these marine deposits are capped by cemented gravels about 30 m thick that reach up to 308 m a.s.l. In very small accessible exposures of the upper part of these gravels no marine macrofauna or ichnofossils were found. The gravel lithofacies characteristics comply

with a littoral environment, although a fluvial origin cannot be firmly excluded. Based on the above, and given the flat morphology of the gravel-capped top of the interfluve and the resemblance to well-defined coastal terrace remnants (CTRs) in the Neos Erineos and Selianitika areas, the 308 m gravel could correspond to a depositional CTR that corresponds to the same highstand as the marine deposits at L22, or a younger highstand.

A small N-dipping fault traverses the 308 m possible CTR and downthrows it to 300 m, whereas at L22 another N-dipping fault has downthrown the underlying marine nearshore silts by a few metres (less than 10). According to Poulimenos (1993, 2000), this fault is the NW tip of a much longer, NW-SE trending, N-dipping secondary fault zone that continues all the way to Aigion. This fault zone passes along FZ2 and coincides with the Koukouvelas and Doutsos (1996) trace of the western part of the Aigion fault (drawn in pink in Figure 1d). Abrupt lithological changes and distinct anomalies in the morphology of the interfluve in the area between L20 and L22 (saddles alternating with highs) suggest faulting. The strikes of probable faults traced in Figure 2b in this area (collectively labelled "FZ1") are approximate, as in all other cases of poor outcrop or/and lack of laterally extensive geomorphic signature. Displacements are possibly minor at L21, considering that in an (inferred) graben structure the marine deposits of L22 were not observed. Between L19 and L20, the interfluve exhibits a down-step of 108 m. As with the 60 m step across FZ2, we do not know how much of this elevation difference may be due to displacement by "FZ1", since this could be the area of the highstand shoreline of the L22 marine sequence. I.e., part of the interfluve down-stepping may well be the result of marine erosion.

Moving to lower elevations, a succession of depositional (and erosional?) CTRs and inconclusive benches is found all the way down to the Neos Erineos village (at 108 m a.s.l.). These surfaces are typically underlain by cemented gravel, with terra rossa on them. Fault zones between them are observable in outcrops, and/or suggested by distinct geomorphic anomalies (Poulimenos 1993, 2000; Palyvos *et al.* 2005 and new data from this study). Contrary to the Selianitika area, where lithologies are soft, geomorphic expression of faults in the Neos Erineos area is favoured by the dominance of gravels that are cemented to a variable extent.

Marine macrofauna is generally restricted to sands and silts below the gravels that are exposed in the SE part of the coastal range-front. In one case (L23), imprints (casts) of marine bivalves were observed within the latter gravels. Thick *Ostrea* sp. shells, comparable to those at the 218 m fan delta at Selianitika and very rich and diverse macrofauna were found at L33 and L34, in silty and sandy shoreface deposits associated to faulted, correlative CTRs at 180-200 (and possibly 220) m a.s.l. Gravel foresets several meters high can be seen in outcrops of the gravels that underlie the 108 m CTR (a Gilbert-type fan delta of the Phoenix R.; Ghisetti and Vezzani, 2004), e.g. at L23 (Figure 10a).

8.2. Chronological constraints and uplift rate estimate

Just south of L22, at an about 276 m a.s.l., two small pieces of *Cladocora* sp. corals were retrieved from colluvium coming from a remnant of the shallow marine silts farther uphill. U-series dating of these corals yielded an age of 187.5 +12.9 / -

11.6 ka. Considering the anomalous ages by *Cladocora* sp. corals from the same type of sedimentary context at L10 and L11, cross-checking of the reliability of the U-series age at L22 by independent evidence is very desirable. No independent dating evidence exists, and, as at Selianitika, the correlation between successive marine terraces and peaks in the sea-level curve that results from the AUR derived from this age cannot be used as a means to independently validate it, due to faulting. The fact that independent evidence in support of the coral age at L22 is lacking, should be weighted accordingly in the final interpretation.

The only marine highstand within this age range is that of MIS7a, in all the eustatic sea-level curves in Figure 9, except that of Siddall *et al.* (2003), which marginally includes a highstand during MIS6 also. By correlating the marine deposits at L22 to the MIS7a highstand, we obtain an AUR of 1.55-1.65 mm/yr using different curves in Figure 9. Because the elevation of the dated deposits is not the elevation of the actual highstand shoreline, this AUR estimate is a minimum for L22. If the 308 m gravels are considered marine and if we assume that they belong to the same sequence as the marine deposits at L22 (we have not seen their relationship in outcrop), by assigning them to MIS7a, AUR would rise to 1.59-1.68 mm/yr. Because the actual highstand shoreline (the terrace inner edge) is not preserved, and thus its actual elevation is unknown, also the above AUR estimate would be a minimum for L22, but closer to the true value than the AUR from the dated marine deposits. The above values are in agreement with the AUR derived at L11 (and with scenarios 2a/b at Selianitika) but, whether this agreement can be considered an independent validation of the obtained U-series age at L22 depends on the –unknown- amount of throw on FZ1 since the deposition of the L22 marine sequence.

9. DISCUSSION

9.1. The Aravonitsa unconformity and the take-over by the ANELfz

The existence of the Aravonitsa unconformity (AU) suggests an abrupt decrease in rate of rotation about a horizontal axis (tilting). This tilting regards a secondary fault block that lies within the broader Lkfz hangingwall block. The AU thus reflects an abrupt “death” of the secondary faults in the hangingwall of the Lkfz that were responsible for the tilting of this secondary block. This event dates within the early part of MIS10, i.e. sometime between ~390 and ~350 ka BP, preferably in the earlier part of this period. It was followed shortly after by net uplift of the broader Lkfz hangingwall, which resulted in the formation of MIS9 (p3 on the Aravonitsa plateau) and younger marine terraces. A possible indication that net uplift may have initiated before MIS9 (i.e. within MIS10), is the erosion of the upper part of the p1 lacustrine foresets (the alternative to uplift being lake-level fall). Assuming a constant rate of regional uplift, initiation of net uplift in the study area implies an increase of the uplift on the ANELfz. Presumably, this resulted from the ANELfz taking up the strain accommodated by the de-activated secondary faults at the Lkfz hangingwall block, in combination with a decrease of hangingwall subsidence rate on the Lkfz. This event (the ANELfz taking up more strain and causing net uplift) is referred to as “take-over by the ANELfz” in the following. It may be the result either of migration of fault activity from the Lkfz to a young, growing ANELfz or, localisation of activity

on an ANELfz that was a large structure already and was previously “co-existing” with the Lkfz (see model by Collier and Jones 2004). In the latter scenario, uplift by the ANELfz would have kept the Lkfz hangingwall block subsidence rate at low values, providing an explanation for the lack of thick Gilbert deltas in this part of the Rift (as opposed to the hangingwall of the PMfz farther East; Figure 1d).

The formation of the AU and the take-over by the ANELfz, appear to coincide temporally with the formation of an unconformity that Bell *et al.* (2008) report in a broad offshore area East of Aigion. According to Bell *et al.* (2008), this unconformity dates between 300-400 ka. This coincidence suggests that the take-over by the ANELfz is probably part of an evolutionary event that affected the entire western part of the Corinth Rift, or at least, a large area therein.

9.2. Uplift rate estimates interpretation

Average uplift rate (AUR) estimates were obtained at four different locations and they refer to four different time spans (Figure 13). AUR estimates based on non independently validated U-series ages in two of the four locations (Neos Erineos, Selianitika), are subject to an unknown amount of uncertainty and are depicted with gray color in Figure 13. In the overall interpretation of the AUR estimates from different locations, we need to consider: a) the uncertainties involved in each of these estimates, b) the context of the recently active, secondary fault zones in the footwall block of the ANELfz and their effect on the spatial and temporal variation of local AURs, c) uncertainties about the secondary fault zones (throws, variation of slip rate with time), d) the distance of AUR estimation locations from the main surface trace of the ANELfz (consideration of possible effects of broad-scale footwall block back-tilting), and, e) the possibility that AURs referring to different periods may record changes of uplift rate with time, in the context of the recent take-over by the ANELfz. Locally, uplift rate may change with time also due to temporal variation of slip rate of secondary faults in the ANELfz footwall.

By “recently active” in (b) above, we refer to secondary fault zones hosting displacements after the deposition/formation of the oldest marine deposits/terrace used for the derivation of AURs (i.e. after MIS9). Figure 14a schematically depicts the effect of such secondary fault zones, which is a discontinuous and differential field of uplift (Figure 14b). In this tectonic context, we cannot assume a pattern of regularly increasing uplift rate (UR) towards the ANELfz. The regular increase in UR that is predicted by theoretical dislocation models (e.g. King *et al.* 1988; Armijo *et al.* 1996; Cianetti *et al.* 2008) at an idealised footwall block (without secondary fault zones), is depicted schematically by the dashed line in Figure 14b. The AUR estimates that better approximate the idealised UR pattern (drawn with filled circles in Figure 14b), should be those that are more useful for the estimation of the slip rate on the ANELfz. If the context of secondary fault zones is ignored or underestimated, erroneous conclusions can easily be reached. E.g., a small local AUR referring to a secondary downthrown block within the broader ANELfz footwall block (e.g. “S” in Figure 14a) may be wrongly considered characteristic of the latter, leading to underestimation of the true strain rate accommodated by the ANELfz. Or, a small AUR from such a secondary fault block, if obtained from a young marine terrace

remnant or deposits, may lead to false inference of reduction of UR with time when compared to local AURs from older marine terraces or deposits farther inland.

If we consider the most conservative AUR estimate at Selianitika (1.11-1.21 mm/yr, “scenario 1” at L31) as the correct one, we end up with a local AUR for the last 125 kyr that is smaller than the 240 kyr AUR estimate at L11 (1.71-1.85 mm/yr); Figure 13. Rather than reflecting a decrease of UR with time, this difference in AUR could equally well (and perhaps, much more likely) reflect the fact that the 152-156 m coastal terrace remnant (CTR) lies on a secondary, downthrown fault block in between secondary faults near the main trace of the active ANELfz. In Figure 14a, the location of the Selianitika terraces would correspond to the block labelled “S”. The same goes for the 125 kyr estimate from “Scenarios 2a/b” at Selianitika (L32), which is still smaller than the 240 kyr AUR at L11, possibly reflecting minor slip on FZ2, and non visible faults between FZ2 and L32. Conversely, if we were to attempt dating a terrace remnant low in the Neos Erineos CTR staircase, considering the multitude of secondary faults that have affected this area after the formation of marine terraces, we would expect lower AUR estimates than at L22, unless all intervening faults died before the deposition/formation of the marine deposits/terrace used for AUR estimation.

Increase of UR with time, during the earlier stages of net uplift at least, is probable in the study area. Take-over by the ANELfz does not preclude the Lkfz still hosting some subsidence after net uplift started, unless we assume that the Lkfz “died” abruptly. This assumption would be arbitrary, considering the lack of relevant data. If instead, subsidence on the Lkfz has been dying out progressively, AURs from marine deposits or terraces dating close to the time of initiation of uplift (~330 ka or somewhat earlier) would underestimate the UR in more recent periods.

The AUR obtained at L11 for the last 240 kyr (1.71-1.85 mm/yr) is substantially higher than that at the Aravonitsa plateau (1.47-1.61 mm/yr) for the last 330 kyr (Figure 13), in agreement with the hypothesis of increasing UR with time during early periods of uplift. Yet, uncertainty is involved in the comparison of AUR estimates at L11 with those on the Aravonitsa plateau, because the estimate at Aravonitsa is minimum-limiting. So is the estimate at L11, but this is not a problem for the above comparison: if a minimum estimate at L11 is higher than the true AUR at Aravonitsa, the true AUR at L11 would certainly be higher. So the question gets down to how much smaller is the minimum AUR estimate at Aravonitsa compared to the true AUR, i.e. whether erosion of the upper part of p3 has been more than we have allowed for in our calculations or not. We have allowed for up to 20 m higher elevation for p3, by considering the highest elevation of the plateau rather than the elevation of the highest occurrence of p3 (which in reality is 500 m a.s.l.). Considering the uncertainty involved in the above, increase of UR between MIS9 and MIS7e is likely, but not proven.

The available data, do not allow for a robust check of whether post-MIS7e UR has been more or less stable (or not). The AUR estimate at L32 (1.66-1.79 mm/yr, from Selianitika scenarios 2a/b) cannot firmly establish stability or increase of UR since MIS7e. First, because it relies on geological assumptions that require more data to be proven (correspondence of the relatively warmest fauna in the study area to MIS5e) and second, due to lack of data on the throws on FZ1, FZ2 and possible secondary faults between FZ2 and L32. In specific, data on the throws that accumulated after the deposition of the dated marine deposits in each case.

A way to firmly establish increase of uplift rate with time along the Selianitika transect, would be to –somehow- date the marine gravel at 348 m, which lie on the footwall of FZ2. Or , to –somehow- date the CTRs at 260 or 248 m in order to test the hypothesis that they may correspond to the landward part of a MIS5e terrace that has been dissected by secondary faults into different CTRs that have been downthrown to successively lower elevations, down to 218 m (where scenarios 2a/b place a MIS5e CTR). In such a case, AUR during the last 125 kyr would be as high as 2.0-2.1 mm/yr at the 260/248 m CTR area, and higher on the FZ2 footwall block, if FZ2 has hosted displacement after MIS5e.

Summing things up, with the available data, the local AUR of 1.71-1.85 mm/yr (close minimum) obtained at L11 from nannoplankton provides at the moment the most reliable approximation of uplift rate at the ANELfz footwall block (dashed line in Figure 14b), at the longitude of the study area. At L11, the effects of secondary fault zones like FZ1 and FZ2 are avoided, as well as the uncertainties about the non cross-checked AUR estimate at L22 or scenarios 2a/b at Selianitika. The estimated AUR at L11 compares well with minimum AUR estimates of ~1.6-1.8 mm/yr obtained from both Pleistocene and Holocene marine deposits and coastal landforms farther NW, where, at the fastest-uplifting areas, present-day AUR may be expected to be higher than at the longitude of Aravonitsa.

Attempts to translate the AUR estimate at L11 to slip rate on the ANELfz, should take into account the distance from the main trace of the ANELfz, and also the fact that uplift rate may contain also a component of broader-scale uniform ("regional") uplift (e.g. Collier et al. 1992; Stewart and Vita-Finzi 1996; Armijo *et al.* 1996; Westaway 2002; Leeder *et al.* 2003). Because the AUR at L11 is a time-averaged estimate for the last 240 kyr, it encompasses periods close to the time of initiation of net uplift, when the uplift rate may have been smaller than today. That is, present-day uplift rate at L11 could be slightly higher at present, and consequently, also the uplift rate closer to the ANELfz.

10. CONCLUSIONS

Structural complexity, intense erosion and a lack of datable material at key locations makes the geomorphic and stratigraphic record of Middle-Late Pleistocene coastal uplift in the study area a fragmentary one. Even so, it is the record that so far provides the clearest information in the area between Aigion and the western termination of the Corinth Rift (Mount Profitis Elias) regarding (a) average coastal uplift rates in late Middle-Late Pleistocene timescales (the last 240 kyr) and (b) the timing of the take-over by the presently active coastal fault zone (ANELfz), and of the initiation of net uplift of the part of the rift fill that accumulated on the hangingwall block of the previously dominant fault zone (Lkfz).

An angular unconformity within the uplifting rift fill, corresponds to abrupt slow-down (or termination) of secondary fault block rotation within the broader hangingwall block of the Lkfz. Based on biostratigraphic correlations of relevant marine deposits with nannoplankton biozones and on stratigraphic considerations, this unconformity dates sometime within the early part of MIS10 (~390 to ~350 ka BP, preferably in the earlier part of this period). Net uplift, driven by the ANELfz taking

over from the Lkfz, initiated shortly after, resulting to the formation of MIS9 and younger marine terraces. Considering that recent studies identify a ~300-400 ka unconformity in a wide offshore area East of Aigion, the take over by the ANELfz could be part of an evolutionary event that affected the entire western part of the Corinth Rift (or, a large area therein).

Dating attempts by the U-series method were made in conjunction with nannoplankton analyses, in order to obtain uplift rate estimates. Stratigraphic constraints and comparisons with calcareous nannofossil analyses, verify that U-series ages of material (incl. corals) from loose (non-cemented) clastic deposits cannot be considered reliable *a priori*, due to open-system behaviour of U-series nuclides, and that validation by independent evidence is necessary. This implies that also the non independently validated U-series ages that have been obtained by different workers (including our group) from corals in similar geologic contexts farther West of the study area, should perhaps be considered "suspect" until more data become available.

Time-averaged estimates of coastal uplift rate (AUR) were obtained at four locations. They refer to different time spans and may record changes (increase) of uplift rate with time, in the context of the recent take-over by the ANELfz. However, the uncertainties in the available data do not allow for a robust test of this hypothesis.

The local AUR estimated at the Aravonitsa plateau area (1.74-1.85 mm/yr, Location 11), is at the moment the only estimate that (a) allows for good approximation of the uplift rate at the ANELfz footwall block (and not just a of secondary fault block within it) at the longitude of Aravonitsa and (b) is based on robust dating evidence from calcareous nannoplankton. The AUR estimate at Aravonitsa refers to a location 3.8 km away from the trace of the ANELfz, and thus it may be somewhat smaller than the uplift rate that would be observed closer to the ANELfz, if secondary faults were not accommodating collapse of the edge of the ANELfz footwall block. Furthermore, being a time-averaged estimate for the last 240 kyr, it encompasses periods close to the time of initiation of net uplift, when the uplift rate may have been smaller than today. That is, present-day uplift rate at Aravonitsa could be slightly higher at present, and perhaps substantially higher closer to the ANELfz.

11. ACKNOWLEDGEMENTS

This study was carried out in the frame of Workpackage 2 (Long-term deformation) of the "3HAZ Corinth" E.U. research project 004043 (GOCE)-3HAZ-Corinth. We warmly thank E. Lemeille for her help in the search for corals and J. Young (Natural History Museum London) for useful discussion on the morphology of *Emiliania huxleyi* early representatives. We appreciate greatly the constructive and thorough reviews of the original manuscript by Mary Ford (Ec. Nat. Sup. de Geol., CRPG, Nancy) and an anonymous Reviewer, and the editorial support by J. Walsh (UC Dublin).

12. REFERENCES

Ambraseys NN, Jackson JA. 1997. Seismicity and strain in the Gulf of Corinth (Greece) since 1694. *J. Earthquake Eng*. **1**: 433-474.

Ahagon N, Tanaka Y, Ujiie H. 1993. Florisphaera profunda, a possible nannoplankton indicator of late Quaternary changes in sea-water turbidity at the northwestern margin of the Pacific. *Marine Micropaleontology* **22**: 255-273.

Armijo R, Meyer B, King GCP, Rigo A, Papanastassiou D. 1996. Quaternary evolution of the Corinth Rift and its implications for the Late Cenozoic evolution of the Aegean. *Geophys. J. Int.* **126**: 11–53.

Avallone A, Briole P, Agatza-Balodimou A-M, Billiris H, Charade O, Mitsakaki C, Nercessian A, Papazissi K, Paradissis D, Veis G. 2004. Analysis of eleven years of deformation measured by GPS in the Corinth Rift Laboratory area. *C.R. Geoscience*, **336**: 4/5, 301-311, doi:10.1016/j.crte.2003.12.007.

Bardaji T, Dabrio CJ, Goy JL, Somoza L, Zazo C. 1990. Pleistocene fan deltas in southeastern Iberian Peninsula: sedimentary controls and sea-level changes. In: *Coarse-grained Deltas* (Eds. A. Colella & D.B. Prior), IAS Spec. Publ.**10**, 129-151.

Bell RE, McNeill LC, Bull JM, Henstock TJ. 2008. Evolution of the offshore western Gulf of Corinth. *Bulletin of the Geological Society of America* **120 (1-2)**: 156-178. doi: 10.1130/B26212.1

Bernard P, Lyon-Caen H, Briole P, Deschamps A, Pitilakis K, Manakou M, Boudin F, Berge C, Makropoulos K, Diagourtas D, Papadimitriou P, Lemeille F, Patau G, Billiris H, Castarède H, Charade O, Nercessian A, Avallone A, Zahradnik J, Sacks S, Linde A. 2006. Seismicity, deformation and seismic hazard in the western rift of Corinth: New insights from the Corinth Rift Laboratory (CRL). *Tectonophysics* **426**: 7-30. doi:10.1016/j.tecto.2006.02.012

Bischoff JL, Fitzpatrick JA. 1991. U-series dating of impure carbonates: an isochron technique using total-sample dissolution. *Geochimica et Cosmochimica Acta* **55**: 543-554.

Briole P, Rigo A, Lyon-Caen H, Ruegg J, Papazissi K, Mitsakaki C, Balodimou A, Veis G, Hatzfeld D, Deschamps A. 2000. Active deformation of the Corinth Rift, Greece: Results from repeated GPS surveys between 1990 and 1995. *J. Geophys. Res* **105**(B11): 25,606-25,626.

Brooks M, Ferentinos, G. 1984. Tectonics and sedimentation in the Gulf of Corinth and the Zakynthos and Kefallinia channels, western Greece. *Tectonophysics* **10**1: 25– 54.

Burbank DW, Anderson RS. 2001. *Tectonic Geomorphology*. Blackwell science, 274 pp.

Chappell J, Shackleton NJ. 1986. Oxygen isotopes and sea-level. Nature **324**: 137-140.

Cianetti S, Tinti E, Giunchi C, Cocco M. 2008. Modelling deformation rates in the western Gulf of Corinth: rheological constraints. *Geophys. J. Int.* **174**:2, 749-757. doi: 10.1111/j.1365-246X.2008.03845.x

Collier R, Jones G. 2004. Rift sequences of the Southern Margin of the Gulf of Corinth (Greece) as Exploration / Production Analogues. Search and Discovery (AAPG): article #50007(2004).

Collier REL, Leeder MR, Rowe RJ, Atkinson TC. 1992. Rates of tectonic uplift in the Corinth and Megara basins, central Greece. *Tectonics* **11:** 1159–1167.

Collier REL, Thompson J. 1991. Transverse and linear dunes in an Upper Pleistocene marine sequence, Corinth Basin, Greece. *Sedimentology* **38**: 1021-1040.

Dart CJ, Collier REL, Gawthorpe RL, Keller JVA, Nichols G. 1994. Sequence stratigraphy of (?)Pliocene-Quaternary synrift, Gilbert-type fan deltas, northern Peloponnesos, Greece. *Mar. Petrol. Geol*. **11**: 545-560.

De Martini P-M, Pantosti D, Palyvos N, Lemeille F, McNeill L, Collier REL. 2004. Slip rates of the Aigion and Eliki faults from uplifted marine terraces, Corinth Gulf, Greece. *Comptes Rendus Geoscience* **336**(4-5): 325-334. doi: 10.1016/j.crte.2003.12.006

Dia AN, Cohen AS, O'Nions RK, Jackson JA. 1997. Rates of uplift investigated through ^{230}Th dating in the Gulf of Corinth (Greece). *Chemical Geology* **138**: 171-184.

Doutsos T, Kontopoulos N, Poulimenos G. 1988. The Corinth-Patras Rift as the initial stage of continental fragmentation behind an active island arc (Greece). *Basin Research* **1**: 177-190.

Doutsos T, Poulimenos G. 1992. Geometry and kinematics of active faults and their seismotectonic significance in the western Corinth-Patras rift (Greece). *Journal of Structural Geology* **14**(6): 689-699.

Dufaure J-J, Zamanis A. 1980. Styles neotectoniques et etagements de nivaux marins sur un segment d'arc insulaire, le Peloponnese. *Proc. Conf. Niveux marins et tectonique Quaternaire dans l' aire Mediteraneenne*, 77-107, CNRS, Paris, France.

Durn G. 2003. Terra rossa in the Mediterranean region: parent materials, compositions and origin. *Geologica Croatica* **56**(1): 83-100.

Emery D, Myers KJ. 1996. *Sequence stratigraphy.* Blackwell, Oxford, 297 pp.

Ferentinos G, Papatheodorou G, Collins MB. 1988. Submarine transport processes on an active submarine fault escarpment: Gulf of Corinth, Greece. *Marine Geology* **83**: 43-61.

Flotté N. 2003. Caracterisation structurale et cinematique d'un rift sur detachement: Le rift de Corinthe-Patras, Grece. *These doct.*, 196 pp., Univ. de Paris-Sud.

Flotté N, Sorel D, Muller C, Tensi J. 2005. Along-strike changes in the structural evolution over a brittle detachment fault: example of the Pleistocene Corinth-Patras Rift (Greece). *Tectonophysics* **403**: 77-94. doi:10.1016/j.tecto.2005.03.015

Ford M, Williams EA, Malartre F, Popescu S-M. 2007. Stratigraphic architecture, sedimenttology and structure of the Vouraikos Gilbert-type ffan delta, Guulf of Corinth, Greece. IAS Sp. publ **83**: 49-90.

Frydas D. 1991. Palaookologische und stratigraphische untersuchugen der diatomeen des pleistozans der N. Peloponnes, Griechenland. *Bull. Geol. Soc. Greece* **XXV/2**: 499-513.

Frydas D, Kontopoulos N, Stamatopoulos L, Guernet C, Voltaggio M. 1995. Middle-Late Pleistocene sediments in the northwestern Peloponnesus, Greece. A combined study of biostratigraphical, radiochronological and sedimentological results. *Berliner Gowiss.* **E16**:589-605.

Ghisetti F, Vezzani L. 2004. Plio-Pleistocene sedimentation and fault segmentation in the Gulf of Corinth (Greece) controlled by inherited structural fabric. *Comptes Rendus Geoscience* **336**: 243-249. doi:10.1016/j.crte.2003.12.008

GoldSworthy M, Jackson J. 2001. Migration of activity within normal fault systems: examples from the Quaternary of mainland Greece. *J. Struct. Geol.* **23**: 489-506. doi:10.1016/S0191-8141(00)00121-8

Hatzfeld D, Karakostas V, Ziazia M, Kassaras I, Papadimitriou E, Makropoulos K, Voulgaris,N, Papaioannou C. 2000. Microseismicity and faulting geometry in the Gulf of Corinth (Greece). *Geophys. J. Int.* **141**: 438–456.

Houghton SL, Roberts GP, Papanikolaou ID, McArthur JM. 2003. New 234U-230Th coral dates from the western Gulf of Corinth: implications for extensional tectonics. *Geophysical Research Letters* **30**(19): 2013. doi:10.1029/2003GL018112

Keller E, Pinter N. 1999. *Active tectonics – Earthquakes, uplift and landscape*. Prentice-Hall, 337 pp.

King GCP, Stein RS, Rundle JB. 1988. The growth of geological structures by repeated earthquakes. *J. Geophys. Res.* **93**: 13307-13319.

Keraudren B, Sorel D. 1987. The terraces of Corinth (Greece) – A detailed record of eustatic sea-level variations during the last 500,000 years. *Marine Geology* **77:** 99-107.

Kontopoulos N, Zelilidis A. 1997. Depositional environments of the coarse-grained lower Pleistocene deposits in the Rio-Antirio basin, Greece. In: *Engineering Geology and the Environment* , Marinos, G. C., Koukis, G. C., Tsabaos , S. G. C., (Eds), Proc. Int. Symp., A. A. Balkema, Rotterdam, 199-204.

Koukouvelas I, Doutsos T. 1996. Implications of structural segmentation during earthquakes: the 1995 earthquake, Gulf of Corinth, Greece. *Journal of Structural Geology* **18**(2): 1381-1388.

Lajoie KR, Ponti DJ, Powell CL, Mathieson SA, Sarna-Wojcicki AM. 1991. *Emergent marine strandlines and associated sediments, coastal California: a record of Quaternary sea-level fluctuations, vertical tectonic movements, climatic changes and coastal processes.* In: R.B. Morrison (Ed.), Quaternary Non-Glacial Geology: Conterminous

United States: Geological Society of America Decade of North America Geology, K-2, pp. 190–214.

Lazar B, Enmar R, Schossberger M, Bar-Matthews M, Halicz L, Stein M, 2004. Diagenetic effects on the distribution of uranium in live and Holocene corals from the Gulf of Aqaba. *Geochimica et Cosmochimica Acta* **68**(22): 4583-4593.

Leeder M, McNeill L, Collier R, Portman C, Rowe P, Andrews J, Gawthorpe RL. 2003. Corinth rift margin uplift: New evidence from Late Quaternary marine shorelines. *Geophysical Research Letters* **30**: 1611. doi:10.1029/2003GL017382

Leeder MR, Harris T, Kirkby MJ. 1998. Sediment supply and climate change: implications for basin stratigraphy. *Basin Research* **10**: 7-18.

Lourens L, Hilgen F, Shackleton NJ, Laskar J, Wilson D. 2004. The Neogene Period. In: *A Geological Time Scale* (Gradstein, F. M., Ogg. J. G., Smith, A. G., eds.), Cambridge University Press, Cambridge, 409-440.

Lykousis V, Sakellariou D, Moretti I, Kaberi H. 2007. Late Quaternary basin evolution of the Gulf of Corinth: sequence stratigraphy, sedimentation, fault-slip and subsidence rates. *Tectonophysics* **440**(1-4): 29-51. doi:10.1016/j.tecto.2006.11.007

Lyon-Caen H, Papadimitriou P, Deschamps A, Bernard P, Makropoulos K, Pacchiani F, Patau, G. 2004. First results of the CRLN seismic network in the western Corinth Rift: evidence for old-fault reactivation, *C. R. Geoscience* **336**(4/5): 343-351, doi:10.1016/j.crte.2003.12.004.

Malartre F, Ford M, Williams E. 2004. Preliminary biostratigraphy and 3D geometry of the Vouraikos Gilbert-type fan delta, Gulf of Corinth, Greece. *C.R.Geoscience* **336**: 269-280. doi:10.1016/j.crte.2003.11.016

Massari F, Parea GC. 1988. Progradational gravel beach sequences in a moderate- to high-energy, microtidal environment. *Sedimentology* **35**: 881-913.

McNeill LC, Collier REL. 2004. Uplift and slip rates of the eastern Eliki fault segment, Gulf of Corinth, Greece, inferred from Holocene and Pleistocene terraces. *Journal of the Geological Society of London* **161**: 81-92.

Mercier J, Delibassis N, Gauthier A, Jarrige J-J, Lemeille F, Philip H, Sébrier M, Sorel D. 1979. La neotectonique de l'Arc Egeen. *Revue de Géologie Dynamique et de Géographie Physique* **21**: 67-92.

Ota Y, Pillans B, Berryman K, Beu A, Fujimori T, Miyauchi T, Berger G. 1996. Pleistocene coastal terraces of Kaikoura Peninsula and the Marlborough coast, South Island, New Zealand. *New Zealand Journal of Geology and Geophysics* **39**: 51-73.

Palyvos N, Lemeille F, Sorel D, Pantosti D, Pavlopoulos K. 2008. Geomorphic and biological indicators of paleoseismicity and Holocene uplift rate at a coastal normal fault footwall (western Corinth Gulf, Greece). *Geomorphology* **96**(1-2): 16-38. doi:10.1016/j.geomorph.2007.07.010

Palyvos N, Sorel D, Lemeille F, Mancini M, Pantosti D, Julia R, Triantaphylou M, De Martini P-M. 2007. Review and new data on uplift rates at the W termination of the Corinth Rift and the NE Rion graben area (Achaia, NW Peloponnesus). *Bulletin of the Geological Society of Greece* **XXXX**: 412-424.

Palyvos N, Pantosti D, De Martini P-M, Lemeille F, Sorel D, Pavlopoulos K. 2005. The Aigion-Neos Erineos normal fault system (Western Corinth Gulf Rift, Greece): Geomorphological signature, recent earthquake history and evolution. *Journal of Geophysical Research* **110**(B9): B09302, 15 pp. doi:10.1029/2004JB003165

Papadopoulos G, Vassilopoulou A, Plessa A. 2000. A new catalogue of historical earthquakes in the Corinth Rift, Central Greece: 480 BC – AD 1910, in Papadopoulos, G.A. (ed)., *Historical Earthquakes and Tsunamis in the Corinth Rift, Central Greece*, Nat. Obs. Ath., Inst. of Geodynamics, publ. no. 12, 9-120.

Peirano A, Morri C, Bianchi CN, Aguirre J, Antonioli F, Calzetta G, Carobene L, Mastronuzzi G, Orrù P. 2004. The Mediterranean coral Cladocora caespitosa: a proxy for

past climate fluctuations? *Global and Planetary Change* **40**, 195-200. doi: 10.1016/S0921-8181(03)00110-3

Perch-Nielsen K. 1985. Cenozoic calcareous nannofossils. In: *Plankton Stratigraphy* (Eds. AH.M. Bolli, J.B. Saunders & K. Perch-Nielsen), Cambridge University Press, pp. 427-554.

Perissoratis C, Piper DJW, Lykousis V. 2000. Alternating marine and lacustrine sedimentation during the late Quaternary in the Gulf of Corinth rift basin, central Greece. *Marine Geology* **167:** 391-411. PII: S0025-3227(00)00038-4

Piper DJW, Doutsos T, Stamatopoulos L. 1990a. Quaternary history of the Gulfs of Patras and Corinth, Greece. *Z. Geomorphol.* **34**: 4, 451-461.

Piper DJW, Kontopoulos N, Anagnostou C, Chronis G, Panagos AG. 1990b. Modern fan deltas in the western Gulf of Corinth, Greece. *Geo-Marine Letters* **10**: 5-12.

Poulimenos G. 2000. Scaling properties of normal fault populations in the western Corinth Graben, Greece: implications for fault growth in large strain settings. *J. Struct. Geol.* **22**: 307-322. PII: S0191-8141(99)00152 -2

Poulimenos G. 1993. Tectonics and sedimentation in the western Corinth Graben, Greece. *N. Jb. Geol. Palaont. Mh.* **H10**: 607-630.

Poulimenos G. 1991. *Tectonic analysis and sedimentology of the Western part of the Corinth Rift*. PhD Thesis, Univ. of Patras, 298 pp.

Poulimenos G, Zelilidis A, Kontopoulos N, Doutsos T. 1993. Geometry of trapezoidal fan deltas and their relationship to extensional faulting along the south-western active margins of the Corinth rift, Greece. *Basin Res.*, **5**: 179–192.

Raffi I, Backman J, Fornaciari E, Palike H, Rio D, Lourens L, Hilgen F. 2006. A review of calcareous nannofossil astrobiochronology encompassing the past 25 million years. *Quaternary Science Reviews* **25**: 3113-3137.

Roberts GP, Koukouvelas I. 1996. Structural and seismological segmentation of the Gulf of Corinth fault system : implications for models of fault growth. *Annali di Geofisica* **XXXIX**(3): 619-646.

Rohais S, Eschard R, Ford M, Guillocheau F, Moretti I. 2007. Stratigraphic architecture of the Plio-Pleistocene infill of the Corinth Rift: Implications for its structural evolution. *Tectonophysics* **440**(1-4): 5-28. doi:10.1016/j.tecto.2006.11.006

Shackleton NJ, Baldauf JG, Flores JA et al. 1995. Biostratigraphic summary for Leg 138. In *"Proceedings of the Ocean Drilling Program, Scientific Results"* (Eds Pisias, N.G., Mayer, L.A., Janecek T.R.), **138**, 517-536.

Siddall M, Rohling EJ, Almogi-Labin A, Hemleben C, Meischner D, Schmelzer I., Smeed DA. 2003. Sea-level fluctuations during the last flacial cycle. *Nature* **423** : 853-858. doi:10.1038/nature01690

Sebrier M. 1977. Tectonique recente d'une transversale a l'arc egéen. Le golfe de Corinthe et ses régions périphériques, *These doct.*,137 pp,.Université Paris XI-Orsay,

Sorel D. 2000. A Pleistocene and still-active detachment fault and the origin of the Corinth-Patras Rift, Greece. *Geology* **28**(1): 83-86.

Sorel D, Lemeille F. 2003. Tilting of the Aigion block in the step-over between the Psathopyrgos and Helike active faults (Gulf of Corinth, Greece) recorded by marine terraces. *Corinth Rift Laboratory June 2003 meeting*, Aigion, Abstracts p. 19.

Sorel D, Pantosti D, Lemeille F, Palyvos N, De-Martini P-M. 2005. The step-over between the Eliki and Aigion fault systems: slip transfer and present rates of activity. Report for CNRS project GDR Corinthe n° 234, 13 pp.

Stamatopoulos L, Voltaggio M, Kontopoulos N. 1994. ^{230}Th / ^{238}U dating of corals from Tyrrhenian marine deposits and the Palaeogeographic evolution of the Western Peloponnesus (Greece). *Munster. Forsch. Geol. Palaont.* **76**: 345-352.

Stamatopoulos L, Kontopoulos N, Voltaggio M, Branca M. 2004. Radiochronological data with U/Th method in lagoonal/marine deposits of the NW Peloponnese, Greece. *Bull. Geol. Soc. Greece* **XXXVI:** 1064-1067.

Stefatos A, Papatheodorou G, Ferentinos G, Leeder M, Collier R. 2002. Seismic reflection imaging of active offshore faults in the Gulf of Corinth: their seismotectonic significance. *Basin Res.* **14**: 487-502.

Stewart I., Vita-Finzi C. 1996. Coastal uplift on active normal faults: The Eliki fault, Greece. *Geoph. Res. Lett.* **23**(14): 1853-1856.

Stirling CH, Esat TH, McCulloch MT, Lambeck K. 1995. High-precision U-series dating of corals from western Australia and implications for the timing and duration of the Last Interglacial. *Earth and Planetary Science Letters* **135**: 115-130.

Thompson WG, Goldstein SL. 2005. Open-system coral ages reveal persistent suborbital sea-level cycles. *Science* **308**: 401-404.

Thompson WG, Spiegelman MW, Goldstein SL, Speed RC. 2003. An open-system model for U-series age determinations of fossil corals. *Earth and Planetary Science Letters* **210**: 365-381.

Trikolas K, Koskeridou E, Tsourou T, Drinia H, Alexouli-Livaditi A. 2004a. Pleistocene marine deposits of the Aigialia region (N. Peloponnesus). *Bull. Geol. Soc. Gr*eece **XXXVI**: 826-835.

Van Wagoner JC, Mitchum RM, Campion KM, Rahmanian VD. 1990. Siliciclastic Sequence Stratigraphy in Well Logs, Cores and Outcrop: Concepts for High Resolution Correlation of Time and Facies. *American Association of Petroleum Geologists, "Methods in Exploration" Series*, Tulsa, **7**, 55 pp.

Walker RG. 1990. Facies modelling and sequence stratigraphy. *Journal of Sedimentary Petrology* **60**: 777-786.

Westaway R. 2002. The Quaternary evolution of the Gulf of Corinth, central Greece: coupling between surface processes and flow in the lower continental crust. *Tectonophysics* **348**: 269.318. PII: S0040-1951(02)00032-X

Zecchin M. 2007. The architectural variability of small-scale cycles in shelf and ramp clastic systems: The controlling factors. *Earth-Science Reviews* **84**: 21-55. doi:10.1016/j.earscirev.2007.05.003

Zygoyri V, Verroios S, Kokkalas S, Xypolias P, Koukouvelas IK. 2008. Scaling properties within the Gulf of Corinth, Greece: comparison between offshore and onshore active faults. *Tectonophysics* **453:** 193-210. doi:10.1016/j.tecto.2007.06.011

TABLE AND FIGURE CAPTIONS

Table 1. Results of U-series datings with the total-sample dissolution method, following the procedures of Bischoff and Fitzpatrick (1991). Determination of isotopic composition by alpha spectroscopy. The "Reference" column lists laboratory reference numbers (IJA/CSIC, Barcelona, Spain). The TS606 age does not result from full analysis (extended counts), due to electricity power failure at 2000 minutes. "***" and "****" indicate that sample TS606 was free of ^{232}Th contamination, and that the ^{230}Th/^{232}Th ratio was infinite (respectively).

Reference	sample	Sample type	Elevation (m a.s.l.)	^{238}U (ppm)	^{232}Th (ppm)	^{230}Th/^{232}Th	^{230}Th/^{234}U	^{234}U / ^{238}U	Age (ka)
TS (1006)	Selianitika	*Calcite crust*	140	0.14	0.02	22.239 ±1.614	0.72 ±0.02	1.41 ±0.03	**127.55** +6.4 / -6.1
TS (606)	Selianitika	*Calcite crust*	140	0.17	***	*****	0.65 ±0.05	1.25 ±0.07	**109.2** +13.2 / -11.9
TS (2806)	Aravonitsa Location 11	*Flabellum sp. (coral)*	410	3.7	0.8	98.781 ±7.506	0.95 ±0.02	1.08 ±0.01	**283.6** +40.0/-29.6
4607	Aravonitsa location 10	*Cladocora sp.*	412	2.64	0.4	16.65 ±0.3	0.78 ±0.02	1.03 ±0.01	**161.8** +8.0 / -7.5
5007	Aravonitsa location 10	*Cladocora sp.*	412	2.76	0.19	34.77 ±2.02	0.80 ±0.02	0.98 ±0.01	**177.9** + 10.2 / -9.3
4507	Aravonitsa location 10	*Cladocora sp.*	412	2.84	0.26	28.72 ±1.18	0.84 ±0.03	1.02 ±0.01	**197.3** + 19.0 / -16.2
4907	Aravonitsa location 10	*Cladocora sp.*	412	2.6	0.38	18.57 ±1.02	0.85 ±0.02	1.03 ±0.02	**200.9** + 17.7 / -15. 2
TS (3306)	Neos Erineos	*Cladocora sp.*	276	1.88	0.15	37.385 ±3.104	0.85 ±0.02	1.16 ±0.02	**187.492** +12.9 / -11.6

Figure 1. (a) Location of the Corinth Rift in the broader geographic and geodynamical context. **(b)** The western part of the Corinth Gulf area, with on-land and submarine fault zones. **(c)** structural cross-section along line shown in (b), by Ghisetti and Vezzani (2005). **(d)** Geological sketch map of the onshore part of the western part of the Corinth Gulf Rift. ANELfz: Aigion-Neos Erineos fault zone, Af: Aigion fault, Lkfz: Lakka f.z., Pfz: Psathopyrgos f.z., RPfz: Rion-Patras f.z., Efz: Eliki f.z., PMfz: Pyrgaki-Mamoussia f.z., PE: Mount Profitis Elias peak.

Figure 2. Topography of the Aravonitsa plateau **(a)** and the Neos Erineos-Selianitika area **(b)**, with lithostratigraphic map, faults and possible faults. Fault traces are based on geomorphic or/and geological evidence (where available). Topographic contours taken from 1:5,000 maps of the Hellenic Army Geographical Service (HAGS). White color (0) indicates areas covered by vegetation, colluvium or soil, not allowing identification of the underlying lithology.

0: non-mapped areas**, 1:** Holocene / Late Pleistocene fluvial deposits (or colluvium derived from terra rossa, on Aravonitsa plateau), **2a:** terra rossa (red soil), **2b:** brown soil, **3:** post MIS9 cemented gravel on (on marine terraces: regressive littoral gravel), **4a/b:** MIS7 and younger marine deposits sand/gravel dominated, at Selianitika/Neos

Erineos (respectively), **4c:** post MIS7 fluvial gravel (Selianika, L31), **4d:** post MIS7 fluvial deposits (Selianitika, L31), **5:** transgressive gravel of post MIS9 marine sequences, **6:** post MIS8e alluvial fan deposits, **7:** marine sands, gravel and silts (MIS9 at the Aravonitsa plateau area –parasequences 2 and 3 in the Aravonitsa formation-, MIS7e at location 11), **8a:** lacustrine fan-delta gravel with large-scale cross bedding (MIS10, parasequence 1), **8b:** alluvial fan gravel (belonging to the same fan-delta depositional system as 8a), **8c:** gravel belonging to the same system as 8a/8b, not discriminated, **9:** lacustrine/brackish/marine deposits (Synania formation, MIS10 and older). Occurrences of marine/brackish macrofauna include locations where the fauna was found in colluvium, slid deposits and surfaces of ploughed fields.

Figure 3. (a) The Aravonitsa plateau at ~500-520 m a.s.l. The Aravonitsa formation (Af) is clearly discernible below the surface, above strongly tilted strata of the Synania formation (Sf). **(b)** The deposits of the Af exposed at a vertical cliff at the northern part of the Aravonitsa plateau. Location 1 in Figure 2a, indicated by rectangle in (a). Apparent dips of stratigraphic contacts are given as apparent dip direction / apparent dip. The thickness (approx. 21 m) of the lower parasequence (lacustrine foresets) was calculated from clinometer measurements from a point of known distance from the cliff. For stratigraphic log of the exposed section see Figure 4a. See text for facies descriptions/interpretations and sequence-stratigraphic subdivision. **(c)** Close-up view of area shown with rectangle in (b)

Figure 4. (a) Stratigraphic log of the part of the Aravonitsa formation outcropping at the cliff at location 1 (Figure 3b/c). **(b)** Log of the lower part of parasequence 1 at location 5 (fine-grained foresets). **(c)** Log of section exposed at a roadcut at location 11. The upper part of the section is shown in Figure 8b.

Figure 5. Simplified geological cross-section at the Aravonitsa plateau area (schematic, not to scale). Sf: Synania formation (Lower Sf: MIS10 and older, Upper Sf: MIS10). Af (grey shade): Aravonitsa formation (MIS10-9 and younger). Thick vertical lines indicate parts of the stratigraphy that are exposed in different locations in the study area (discussed in the text).

Figure 6. The angular unconformity within the upper part of the Synania formation (Sf), below the Aravonitsa formation (Af) (Location 4 in Figure 2a). The deposits in the upper Sf and the part of the Af visible in the photo, are mapped in different lithostratigraphic units, but they belong to the same sequence-stratigraphic unit (S1).

Figure 7. (a) Stratigraphic log of the Synania formation (Sf) deposits at location 10, where the oldest known layer with purely marine macrofauna occurs. Marine deposits pass upwards to brackish and then lacustrine deposits without any intervening unconformity, reflecting the salinity fluctuations within the sill-controlled Corinth Gulf. The log comes from an outcrop with strongly tilted (175/30), lower Sf deposits. **(b)** Log of an occurrence of a marine layer within Sf deposits at Ano Zeria, Mount

Profitis Elias area. The marine layer is in all probability correlative to that in (a). **(c)** Log of outcrop with marine layer correlative to that in (b), dated with the U-series method by Sorel *et al.* (2005).

Figure 8. (a) Ploughed field at location 11, where very rich marine malacofauna was found, including *Flabellum* sp. corals that were dated with the U-series method. **(b)** Roadcut 30 m NE of the scraped field shown in (a). The roadcut exposes the upper part of the section shown in Figure 4b. Marine sandy silts with nannoflora marginally within biozone MNN21a, correlate to those on the scraped field shown in (a). **(c)** *Emiliania huxleyi* coccoliths from location 11 (410 m a.s.l.). **(d)** the *Flabellum* sp. corals dated with the U-series method

Figure 9. Average uplift rate estimates at the ANELfz footwall using different sea-level curves. Only scenarios 2a/b are depicted for the Selianitika area (L32), because only these scenarios provide a useful proxy for the uplift rate at the broader ANELfz footwall (rather than on a secondary fault block within it). See text for explanations. The graphical depiction of average uplift rate estimates follows Keller and Pinter (1999).

Figure 10. **(a)** Gravel foresets of the Neos Erineos uplifted marine fan-delta, right below the 108 m terrace at location 23. **(b)** Depositional marine terrace at the Selianitika transect. The terrace is the topset surface of a small gravel fan-delta. The characteristic terra rossa (palaeosoil) is locally preserved, and very thick and large *Ostrea* sp. are found in the topset gravel. **(c, d, e)** The outcrops of marine sands and underlying deposits at location 31 (Selianitika transect).

Figure 11. (a) Geological cross section along the Selianitika transect (profile A in Figure 2b). **(b)** and **(c)** Possible restorations of cross section in (a), in accordance with scenario 2 (see text). The restorations are simplistic in that they do not account for warping and fault block rotations.

Figure 12. Views of calcite crusts within the sands at Location 31 in Figure 10c.

Figure 13. Topographic profiles from Aravonitsa to Neos Erineos and Selianitika (profile traces in Figure 2), with probable configuration of secondary fault zones. Thicker fault traces denote faults with larger displacements and *vice versa*. Profile traces were chosen to follow interfluves, in order to show the morphological steps observed there (due to presence of marine terrace remains or to faulting). Consequently, the spacing of faults and the width of fault blocks is more or less distorted. Local average uplift rate estimates (AURs) referring to different periods are also indicated. Gray color is used to indicate uncertainty introduced by lack of independent cross-checking of U-series ages by other dating methods and, in the case of “Scenario 2” at L32, uncertainty in the involved geological assumptions.

Figure 14. **(a)** Schematic representation of the uplifting footwall block of the ANELfz (the hangingwall block of the Lkfz), and of secondary fault zones on it. Only secondary fault zones shown that are associated with recent displacements (during the last ~330 ka) are shown. Older faults that are probably responsible for a complex structure of tilted secondary fault blocks are not depicted. **(b)** Indicative uplift rate field (pattern) on the ANELfz footwall. The structural complexity introduced by secondary fault zones, results in a discontinuous and differential uplift pattern. Solid circles indicate those uplift rate estimates that better approximate the uplift rate at an idealised ANELfz footwall without secondary faults. The idealised pattern of uplift is shown with a dashed line.

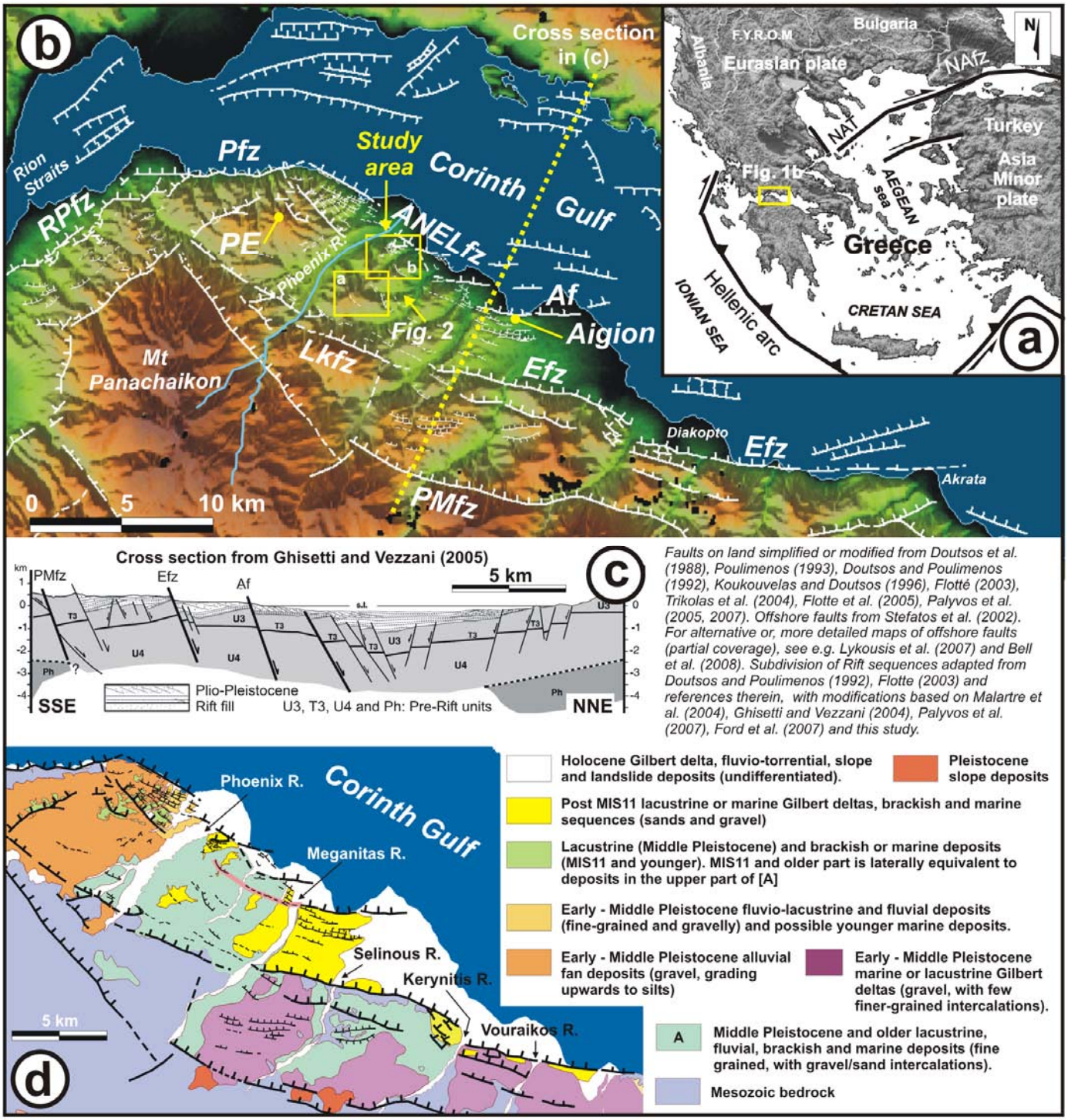
b
Cross section in (c)
Rion Straits
Pfz
Study area
Corinth Gulf
RPfz
PE
ANELfz
Phoenix R.
a
b
Af
Fig. 2
Aigion
Mt Panachaikon
Lkfz
Efz
Diakopto
Akrata
PMfz
0 5 10 km
F.Y.R.O.M
Bulgaria
Albania
Eurasian plate
NAfz
N
NAT
Turkey
Asia Minor plate
Fig. 1b
AEGEAN sea
Greece
Hellenic arc
IONIAN SEA
CRETAN SEA
a
Cross section from Ghisetti and Vezzani (2005)
5 km
c
km
PMfz
Efz
Af
s.l.
T3
U3
U4
Ph
SSE
NNE
Plio-Pleistocene Rift fill
U3, T3, U4 and Ph: Pre-Rift units
Faults on land simplified or modified from Doutsos et al. (1988), Poulimenos (1993), Doutsos and Poulimenos (1992), Koukouvelas and Doutsos (1996), Flotté (2003), Trikolas et al. (2004), Flotte et al. (2005), Palyvos et al. (2005, 2007). Offshore faults from Stefatos et al. (2002). For alternative or, more detailed maps of offshore faults (partial coverage), see e.g. Lykousis et al. (2007) and Bell et al. (2008). Subdivision of Rift sequences adapted from Doutsos and Poulimenos (1992), Flotte (2003) and references therein, with modifications based on Malartre et al. (2004), Ghisetti and Vezzani (2004), Palyvos et al. (2007), Ford et al. (2007) and this study.
Phoenix R.
Corinth Gulf
Meganitas R.
Selinous R.
Kerynitis R.
Vouraikos R.
5 km
d
Holocene Gilbert delta, fluvio-torrential, slope and landslide deposits (undifferentiated).
Pleistocene slope deposits
Post MIS11 lacustrine or marine Gilbert deltas, brackish and marine sequences (sands and gravel)
Lacustrine (Middle Pleistocene) and brackish or marine deposits (MIS11 and younger). MIS11 and older part is laterally equivalent to deposits in the upper part of [A]
Early - Middle Pleistocene fluvio-lacustrine and fluvial deposits (fine-grained and gravelly) and possible younger marine deposits.
Early - Middle Pleistocene alluvial fan deposits (gravel, grading upwards to silts)
Early - Middle Pleistocene marine or lacustrine Gilbert deltas (gravel, with few finer-grained intercalations).
A
Middle Pleistocene and older lacustrine, fluvial, brackish and marine deposits (fine grained, with gravel/sand intercalations).
Mesozoic bedrock

Fig 1

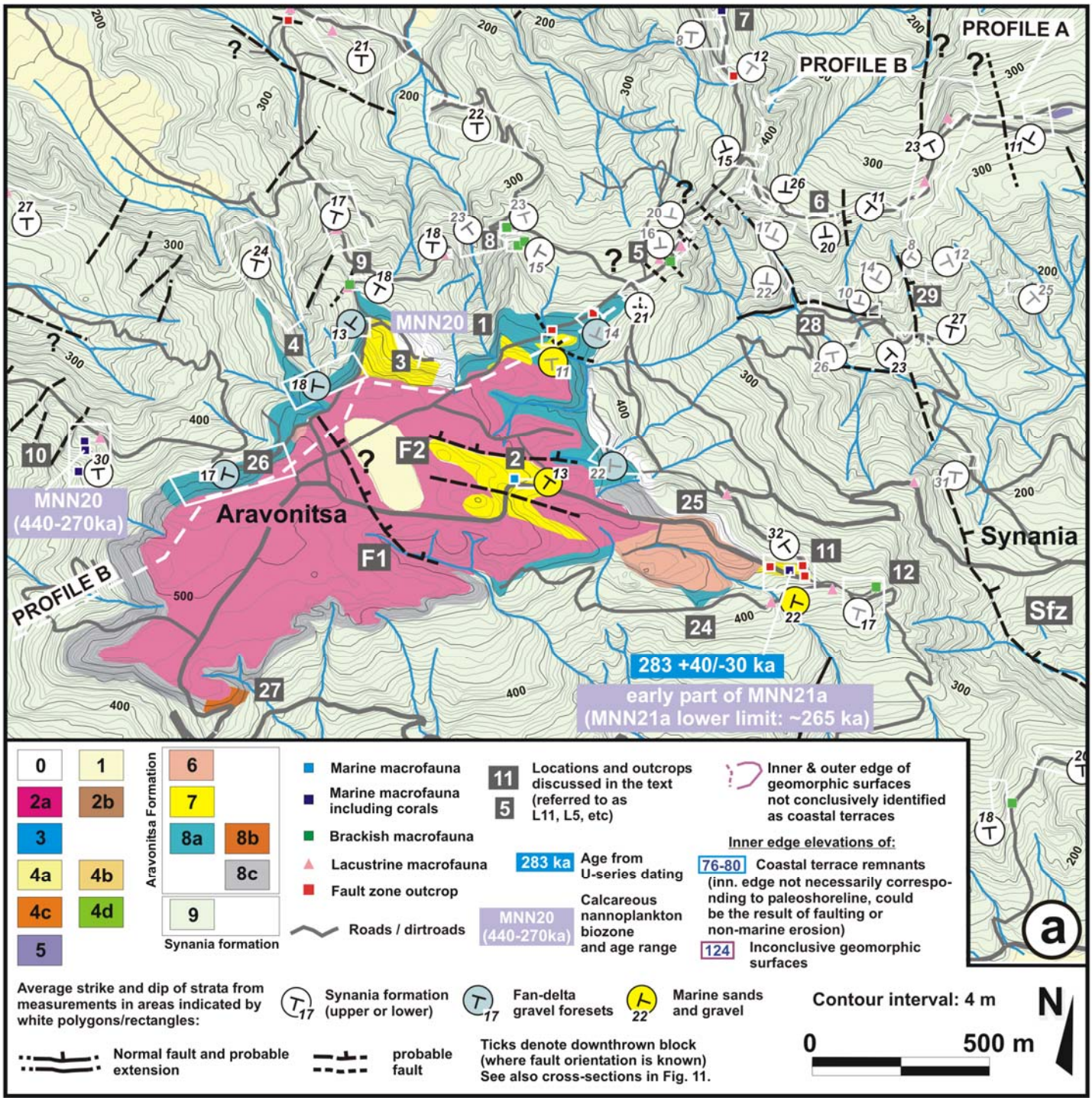
PROFILE A
PROFILE B
MNN20
Aravonitsa
MNN20
(440-270ka)
F1
F2
Synania
Sfz
283 +40/-30 ka
early part of MNN21a
(MNN21a lower limit: ~265 ka)
Aravonitsa Formation
Synania formation
Marine macrofauna
Marine macrofauna including corals
Brackish macrofauna
Lacustrine macrofauna
Fault zone outcrop
Roads / dirtroads
Locations and outcrops discussed in the text (referred to as L11, L5, etc)
Age from U-series dating
Calcareous nannoplankton biozone and age range
Inner & outer edge of geomorphic surfaces not conclusively identified as coastal terraces
Inner edge elevations of:
Coastal terrace remnants (inn. edge not necessarily corresponding to paleoshoreline, could be the result of faulting or non-marine erosion)
Inconclusive geomorphic surfaces
Average strike and dip of strata from measurements in areas indicated by white polygons/rectangles:
Synania formation (upper or lower)
Fan-delta gravel foresets
Marine sands and gravel
Contour interval: 4 m
Normal fault and probable extension
probable fault
Ticks denote downthrown block (where fault orientation is known)
See also cross-sections in Fig. 11.
0
500 m
N
a

Fig 2

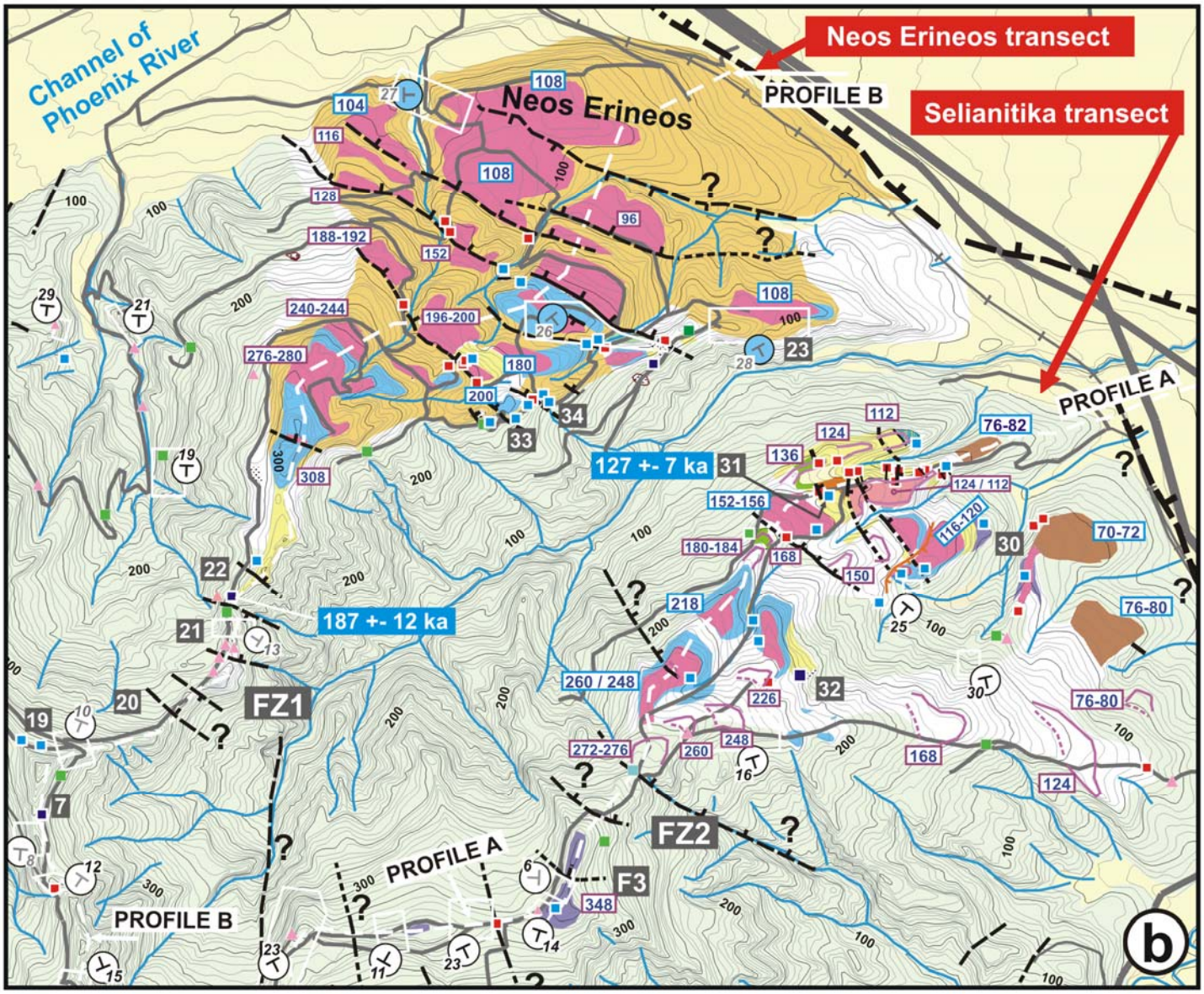
Channel of Phoenix River
Neos Erineos transect
Selianitika transect
Neos Erineos
PROFILE B
PROFILE A
127 +- 7 ka
187 +- 12 ka
FZ1
FZ2
F3
b

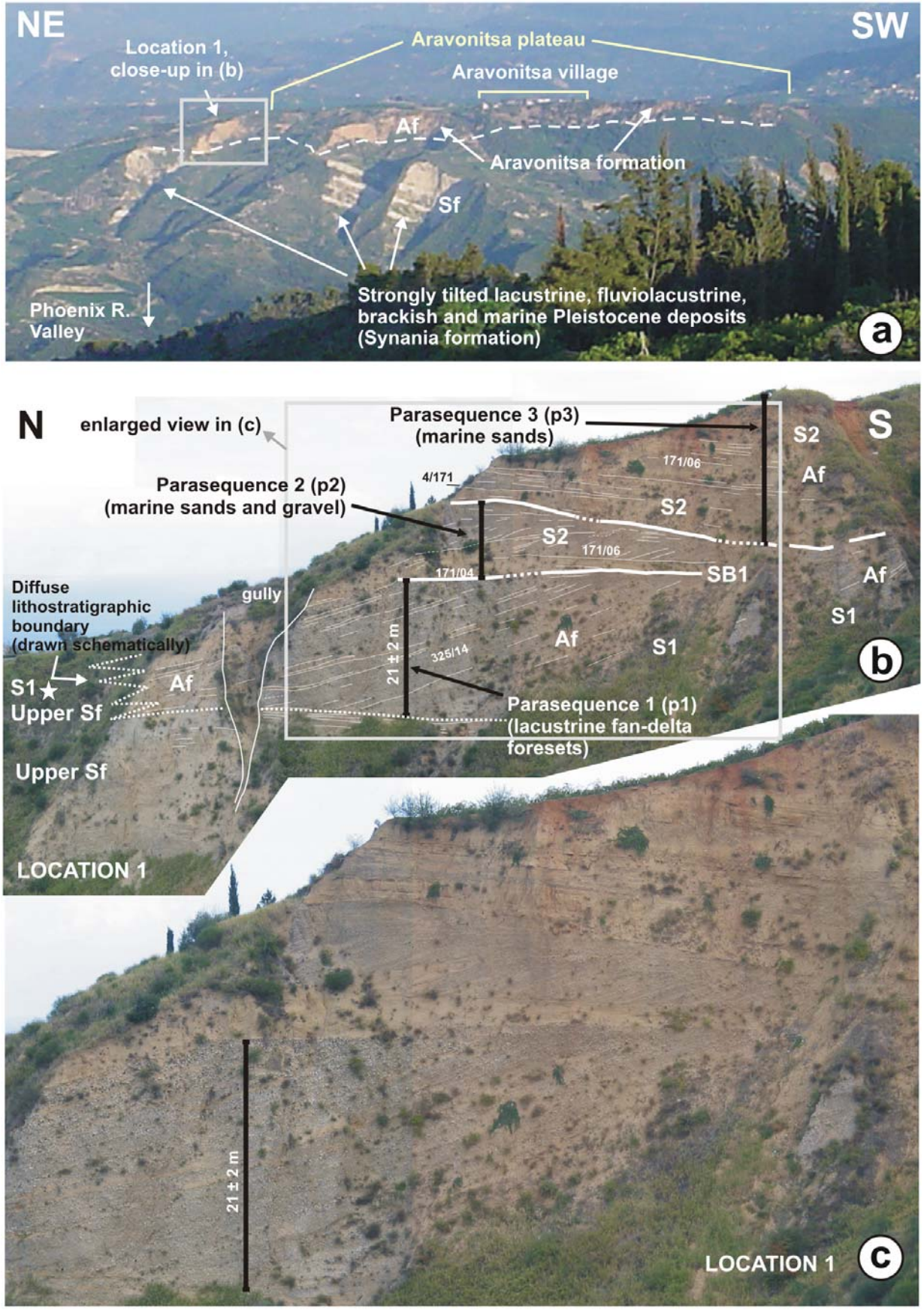
NE
SW
Location 1, close-up in (b)
Aravonitsa plateau
Aravonitsa village
Af
Aravonitsa formation
Sf
Phoenix R. Valley
Strongly tilted lacustrine, fluviolacustrine, brackish and marine Pleistocene deposits (Synania formation)
a
N
enlarged view in (c)
Parasequence 3 (p3) (marine sands)
S2
S
Af
171/06
4/171
Parasequence 2 (p2) (marine sands and gravel)
S2
S2
171/06
171/04
SB1
Af
S1
Diffuse lithostratigraphic boundary (drawn schematically)
gully
21 ± 2 m
325/14
Af
S1
b
S1
Af
Upper Sf
Parasequence 1 (p1) (lacustrine fan-delta foresets)
Upper Sf
LOCATION 1
21 ± 2 m
LOCATION 1
c

Fig 3

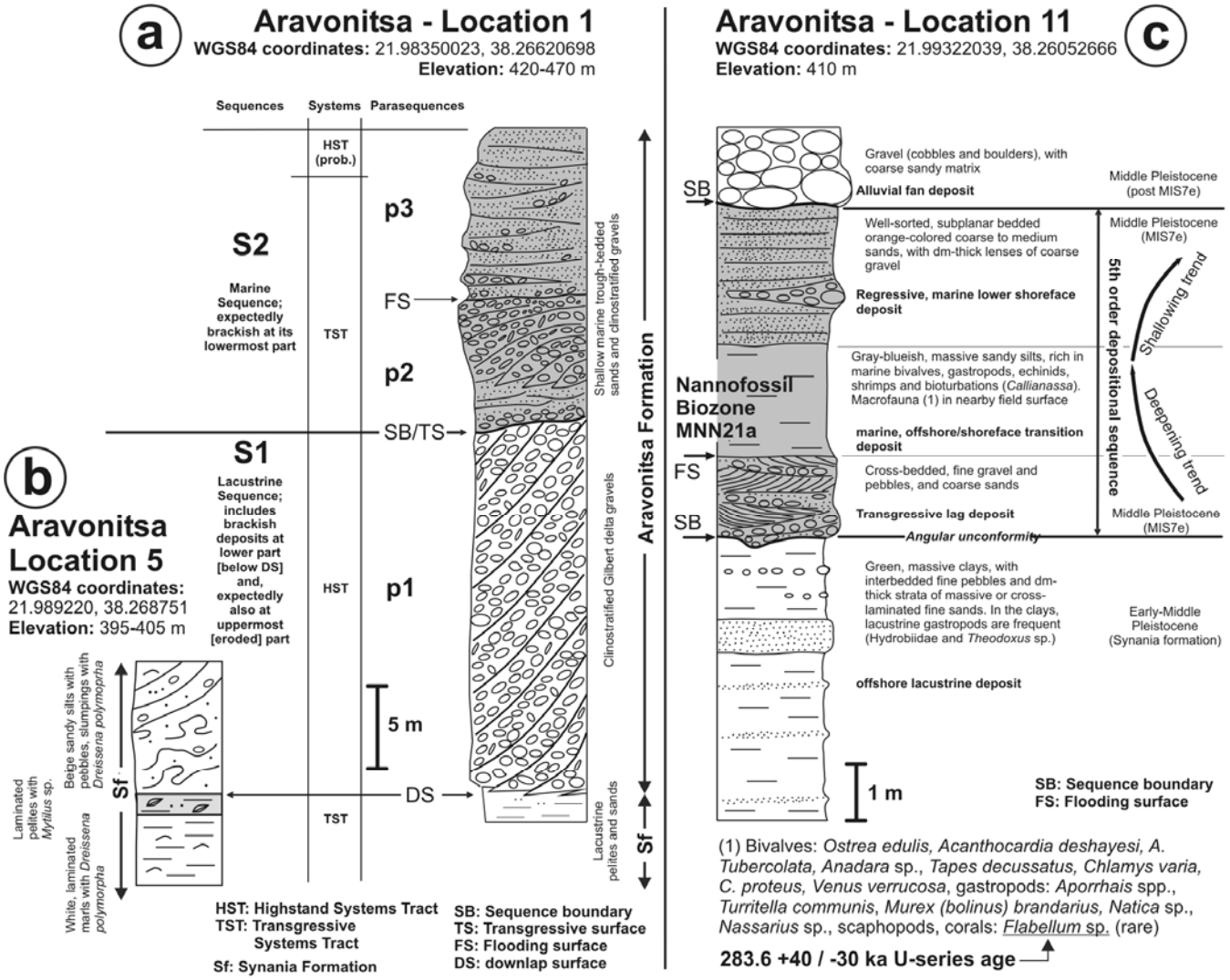
a
Aravonitsa - Location 1
WGS84 coordinates: 21.98350023, 38.26620698
Elevation: 420-470 m
Sequences
Systems
Parasequences
HST (prob.)
S2
Marine Sequence; expectedly brackish at its lowermost part
TST
p3
FS
p2
SB/TS
S1
Lacustrine Sequence; includes brackish deposits at lower part [below DS] and, expectedly also at uppermost [eroded] part
HST
p1
5 m
DS
TST
Shallow marine trough-bedded sands and clinostratified gravels
Clinostratified Gilbert delta gravels
Lacustrine pelites and sands
Aravonitsa Formation
Sf
b
Aravonitsa Location 5
WGS84 coordinates: 21.989220, 38.268751
Elevation: 395-405 m
Laminated pelites with Mytilus sp.
Beige sandy silts with pebbles, slumpings with Dreissena polymorpha
Sf
White, laminated marls with Dreissena polymorpha
HST: Highstand Systems Tract
TST: Transgressive Systems Tract
Sf: Synania Formation
SB: Sequence boundary
TS: Transgressive surface
FS: Flooding surface
DS: downlap surface
Aravonitsa - Location 11
WGS84 coordinates: 21.99322039, 38.26052666
Elevation: 410 m
c
SB
Gravel (cobbles and boulders), with coarse sandy matrix
Alluvial fan deposit
Middle Pleistocene (post MIS7e)
Well-sorted, subplanar bedded orange-colored coarse to medium sands, with dm-thick lenses of coarse gravel
Regressive, marine lower shoreface deposit
Middle Pleistocene (MIS7e)
5th order depositional sequence
Shallowing trend
Deepening trend
Nannofossil Biozone MNN21a
Gray-blueish, massive sandy silts, rich in marine bivalves, gastropods, echinids, shrimps and bioturbations (Callianassa). Macrofauna (1) in nearby field surface
marine, offshore/shoreface transition deposit
FS
Cross-bedded, fine gravel and pebbles, and coarse sands
Transgressive lag deposit
SB
Angular unconformity
Middle Pleistocene (MIS7e)
Green, massive clays, with interbedded fine pebbles and dm-thick strata of massive or cross-laminated fine sands. In the clays, lacustrine gastropods are frequent (Hydrobiidae and Theodoxus sp.)
Early-Middle Pleistocene (Synania formation)
offshore lacustrine deposit
1 m
SB: Sequence boundary
FS: Flooding surface
(1) Bivalves: Ostrea edulis, Acanthocardia deshayesi, A. Tubercolata, Anadara sp., Tapes decussatus, Chlamys varia, C. proteus, Venus verrucosa, gastropods: Aporrhais spp., Turritella communis, Murex (bolinus) brandarius, Natica sp., Nassarius sp., scaphopods, corals: Flabellum sp. (rare)
283.6 +40 / -30 ka U-series age

Fig 4

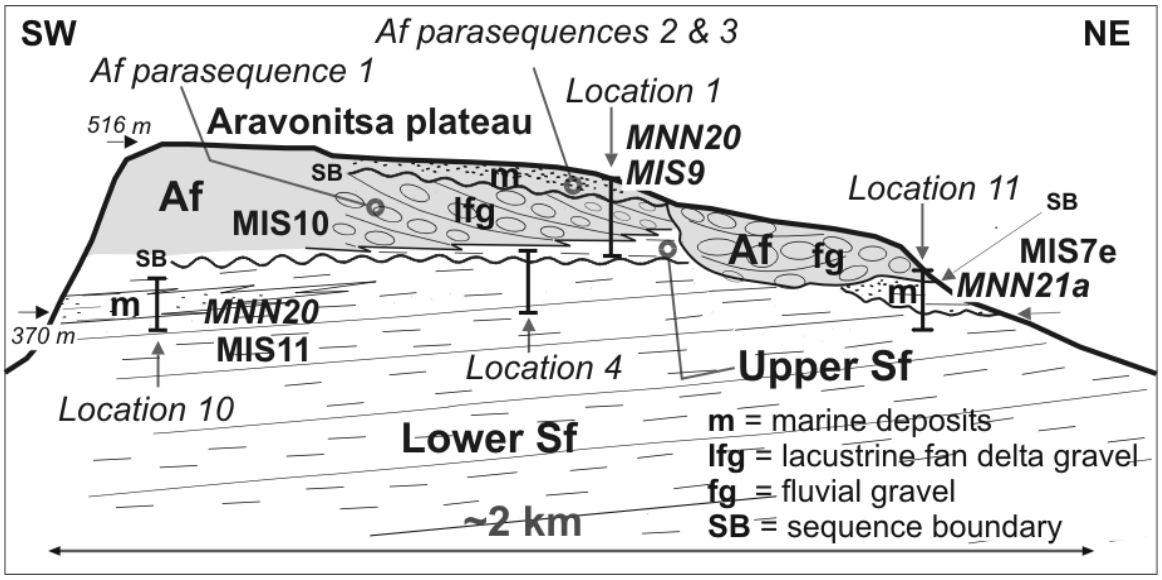
SW
Af parasequences 2 & 3
NE
Af parasequence 1
Location 1
516 m
Aravonitsa plateau
MNN20
MIS9
SB
m
Af
MIS10
lfg
Location 11
SB
SB
Af
fg
MIS7e
MNN21a
m
m
MNN20
370 m
MIS11
Location 4
Upper Sf
Location 10
Lower Sf
m = marine deposits
lfg = lacustrine fan delta gravel
fg = fluvial gravel
SB = sequence boundary
~2 km

Fig 5

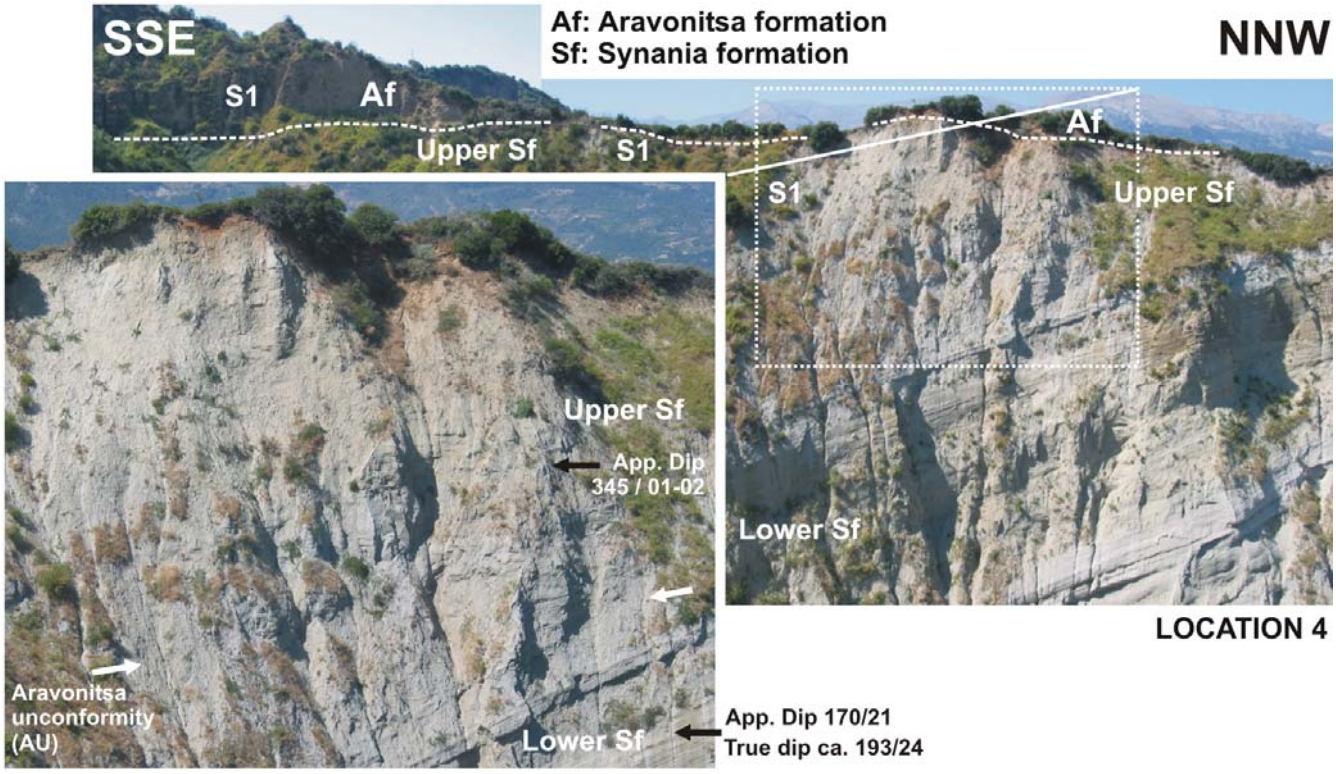
SSE
Af: Aravonitsa formation
Sf: Synania formation
NNW
S1
Af
Upper Sf
S1
Af
S1
Upper Sf
Upper Sf
App. Dip
345 / 01-02
Lower Sf
LOCATION 4
Aravonitsa
unconformity
(AU)
Lower Sf
App. Dip 170/21
True dip ca. 193/24

Fig 6

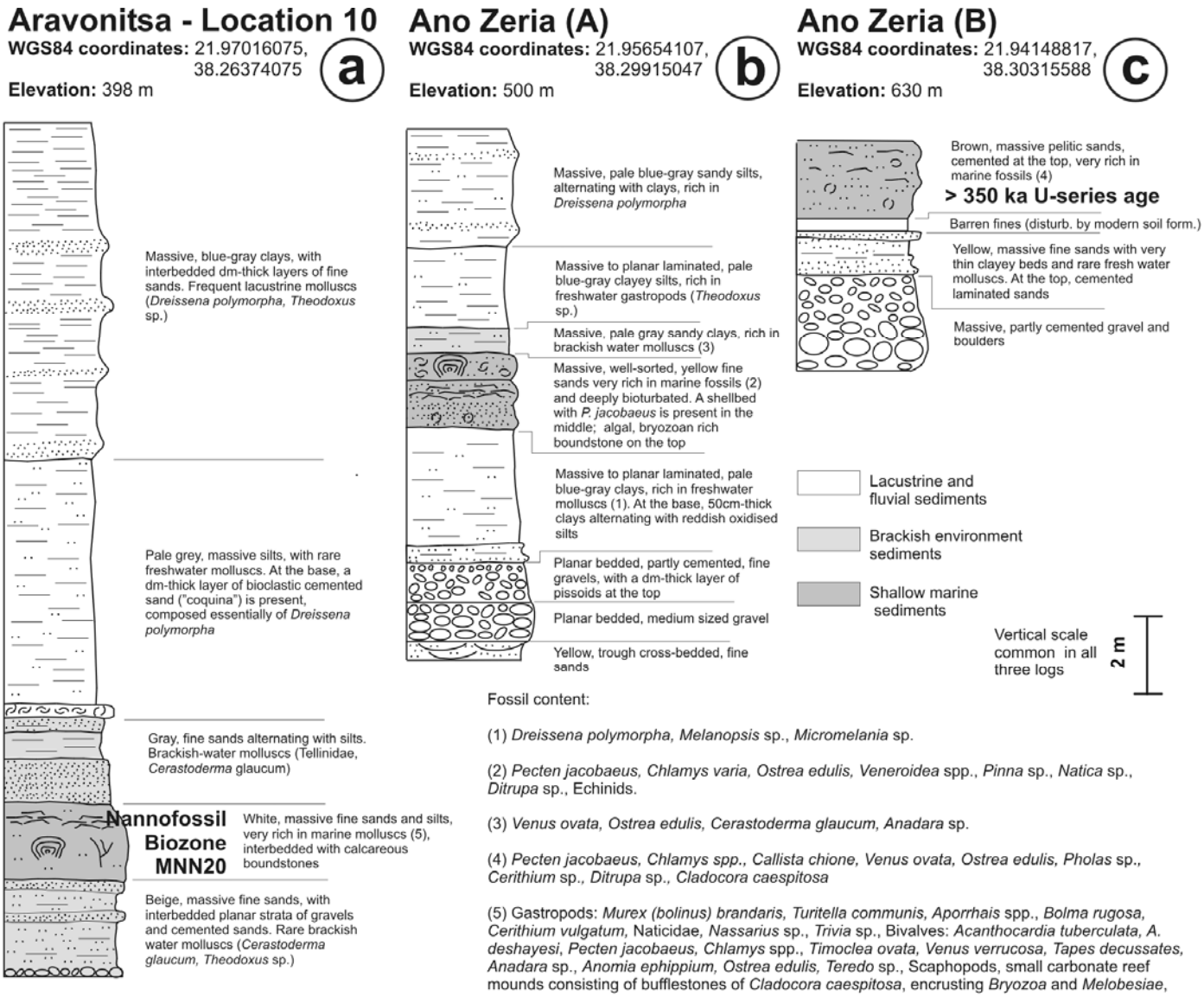
Aravonitsa - Location 10
WGS84 coordinates: 21.97016075, 38.26374075
Elevation: 398 m
a
Massive, blue-gray clays, with interbedded dm-thick layers of fine sands. Frequent lacustrine molluscs (Dreissena polymorpha, Theodoxus sp.)
Pale grey, massive silts, with rare freshwater molluscs. At the base, a dm-thick layer of bioclastic cemented sand ("coquina") is present, composed essentially of Dreissena polymorpha
Gray, fine sands alternating with silts. Brackish-water molluscs (Tellinidae, Cerastoderma glaucum)
Nannofossil Biozone MNN20
White, massive fine sands and silts, very rich in marine molluscs (5), interbedded with calcareous boundstones
Beige, massive fine sands, with interbedded planar strata of gravels and cemented sands. Rare brackish water molluscs (Cerastoderma glaucum, Theodoxus sp.)
Ano Zeria (A)
WGS84 coordinates: 21.95654107, 38.29915047
Elevation: 500 m
b
Massive, pale blue-gray sandy silts, alternating with clays, rich in Dreissena polymorpha
Massive to planar laminated, pale blue-gray clayey silts, rich in freshwater gastropods (Theodoxus sp.)
Massive, pale gray sandy clays, rich in brackish water molluscs (3)
Massive, well-sorted, yellow fine sands very rich in marine fossils (2) and deeply bioturbated. A shellbed with P. jacobaeus is present in the middle; algal, bryozoan rich boundstone on the top
Massive to planar laminated, pale blue-gray clays, rich in freshwater molluscs (1). At the base, 50cm-thick clays alternating with reddish oxidised silts
Planar bedded, partly cemented, fine gravels, with a dm-thick layer of pissoids at the top
Planar bedded, medium sized gravel
Yellow, trough cross-bedded, fine sands
Ano Zeria (B)
WGS84 coordinates: 21.94148817, 38.30315588
Elevation: 630 m
c
Brown, massive pelitic sands, cemented at the top, very rich in marine fossils (4)
> 350 ka U-series age
Barren fines (disturb. by modern soil form.)
Yellow, massive fine sands with very thin clayey beds and rare fresh water molluscs. At the top, cemented laminated sands
Massive, partly cemented gravel and boulders
Lacustrine and fluvial sediments
Brackish environment sediments
Shallow marine sediments
Vertical scale common in all three logs
2 m
Fossil content:
(1) Dreissena polymorpha, Melanopsis sp., Micromelania sp.
(2) Pecten jacobaeus, Chlamys varia, Ostrea edulis, Veneroidea spp., Pinna sp., Natica sp., Ditrupa sp., Echinids.
(3) Venus ovata, Ostrea edulis, Cerastoderma glaucum, Anadara sp.
(4) Pecten jacobaeus, Chlamys spp., Callista chione, Venus ovata, Ostrea edulis, Pholas sp., Cerithium sp., Ditrupa sp., Cladocora caespitosa
(5) Gastropods: Murex (bolinus) brandaris, Turitella communis, Aporrhais spp., Bolma rugosa, Cerithium vulgatum, Naticidae, Nassarius sp., Trivia sp., Bivalves: Acanthocardia tuberculata, A. deshayesi, Pecten jacobaeus, Chlamys spp., Timoclea ovata, Venus verrucosa, Tapes decussates, Anadara sp., Anomia ephippium, Ostrea edulis, Teredo sp., Scaphopods, small carbonate reef mounds consisting of bufflestones of Cladocora caespitosa, encrusting Bryozoa and Melobesiae,

Fig.7

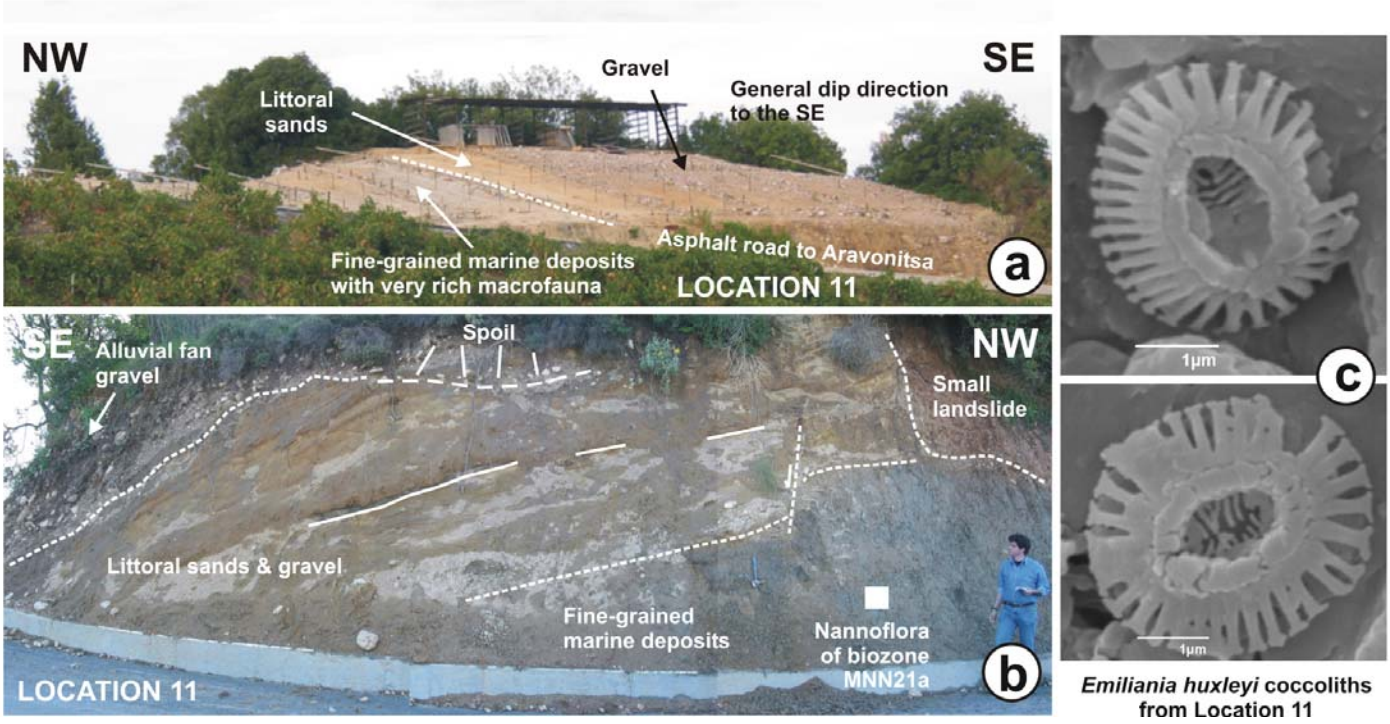
NW
SE
Littoral sands
Gravel
General dip direction to the SE
Fine-grained marine deposits with very rich macrofauna
Asphalt road to Aravonitsa
LOCATION 11
a
SE
Alluvial fan gravel
Spoil
NW
Small landslide
Littoral sands & gravel
Fine-grained marine deposits
Nannoflora of biozone MNN21a
LOCATION 11
b
1μm
c
1μm
Emiliania huxleyi coccoliths from Location 11

Fig. 8

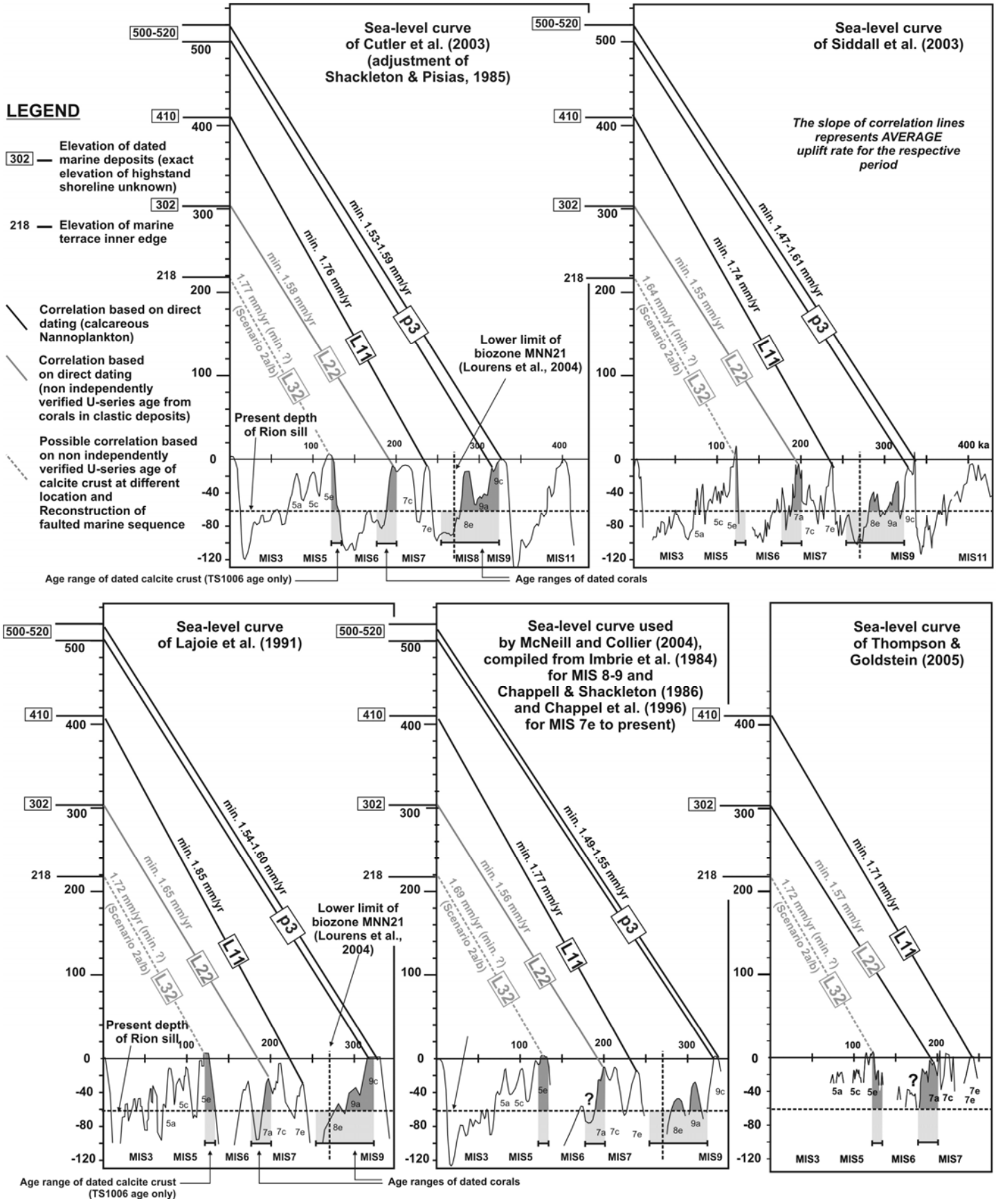
LEGEND
302 — Elevation of dated marine deposits (exact elevation of highstand shoreline unknown)
218 — Elevation of marine terrace inner edge
Correlation based on direct dating (calcareous Nannoplankton)
Correlation based on direct dating (non independently verified U-series age from corals in clastic deposits)
Possible correlation based on non independently verified U-series age of calcite crust at different location and Reconstruction of faulted marine sequence
Sea-level curve of Cutler et al. (2003) (adjustment of Shackleton & Pisias, 1985)
Sea-level curve of Siddall et al. (2003)
The slope of correlation lines represents AVERAGE uplift rate for the respective period
Sea-level curve of Lajoie et al. (1991)
Sea-level curve used by McNeill and Collier (2004), compiled from Imbrie et al. (1984) for MIS 8-9 and Chappell & Shackleton (1986) and Chappel et al. (1996) for MIS 7e to present)
Sea-level curve of Thompson & Goldstein (2005)
Lower limit of biozone MNN21 (Lourens et al., 2004)
Present depth of Rion sill
min. 1.53-1.59 mm/yr
min. 1.76 mm/yr
min. 1.58 mm/yr
1.77 mm/yr (min. ?) (Scenario 2a/b)
min. 1.47-1.61 mm/yr
min. 1.74 mm/yr
min. 1.55 mm/yr
1.64 mm/yr (min. ?) (Scenario 2a/b)
min. 1.54-1.60 mm/yr
min. 1.85 mm/yr
min. 1.65 mm/yr
1.72 mm/yr (min. ?) (Scenario 2a/b)
min. 1.49-1.55 mm/yr
min. 1.77 mm/yr
min. 1.56 mm/yr
1.69 mm/yr (min. ?) (Scenario 2a/b)
min. 1.71 mm/yr
min. 1.57 mm/yr
1.72 mm/yr (min. ?) (Scenario 2a/b)
L11
L22
L32
p3
MIS3
MIS5
MIS6
MIS7
MIS8
MIS9
MIS11
400 ka
Age range of dated calcite crust (TS1006 age only)
Age ranges of dated corals

Fig. 9.

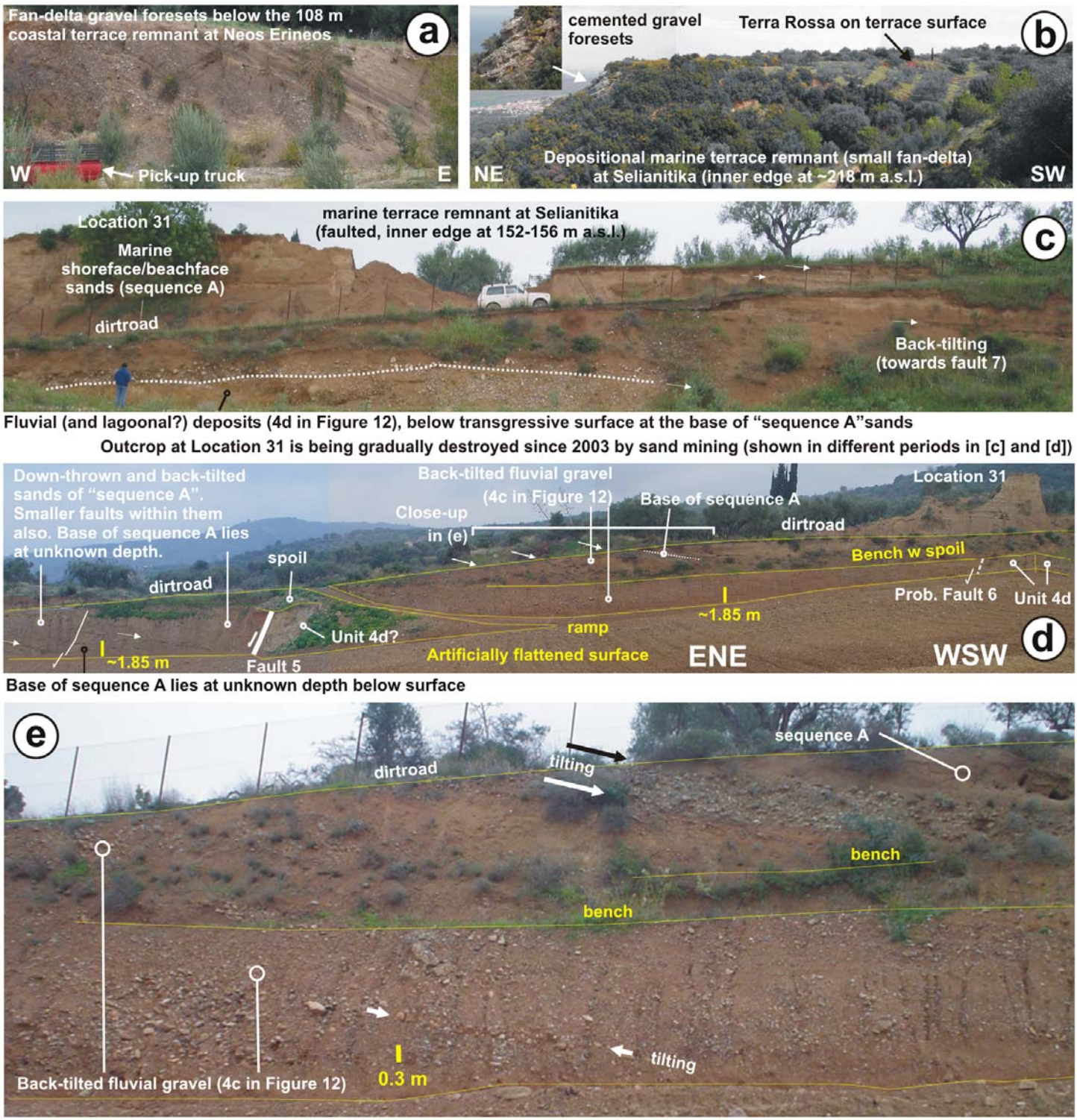

Fluvial (and lagoonal?) deposits (4d in Figure 12), below transgressive surface at the base of "sequence A"sands

Outcrop at Location 31 is being gradually destroyed since 2003 by sand mining (shown in different periods in [c] and [d])

Base of sequence A lies at unknown depth below surface

Fig **10**

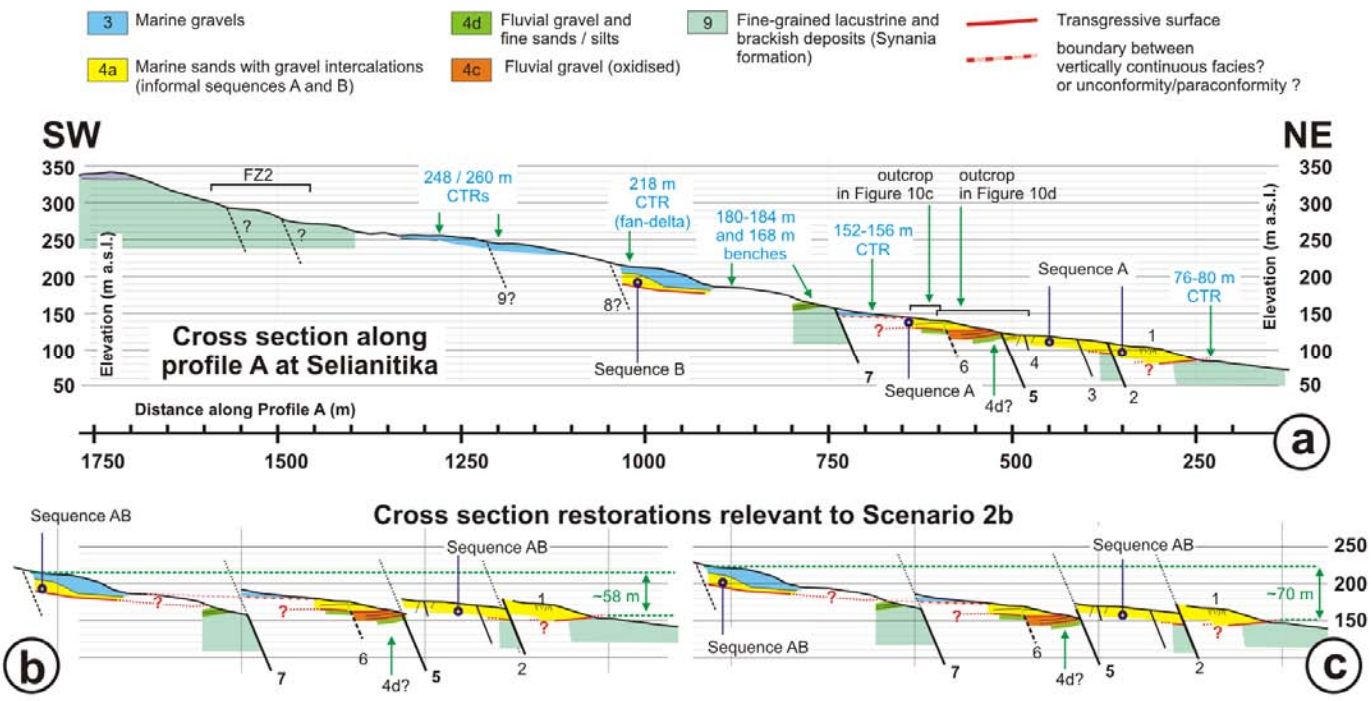
3 Marine gravels
4a Marine sands with gravel intercalations (informal sequences A and B)
4d Fluvial gravel and fine sands / silts
4c Fluvial gravel (oxidised)
9 Fine-grained lacustrine and brackish deposits (Synania formation)
Transgressive surface
boundary between vertically continuous facies? or unconformity/paraconformity ?
SW
NE
Cross section along profile A at Selianitika
Elevation (m a.s.l.)
Distance along Profile A (m)
FZ2
248 / 260 m CTRs
218 m CTR (fan-delta)
180-184 m and 168 m benches
152-156 m CTR
outcrop in Figure 10c
outcrop in Figure 10d
76-80 m CTR
Sequence A
Sequence B
9?
8?
4d?
a
Cross section restorations relevant to Scenario 2b
Sequence AB
~58 m
~70 m
b
c

Fif. 11

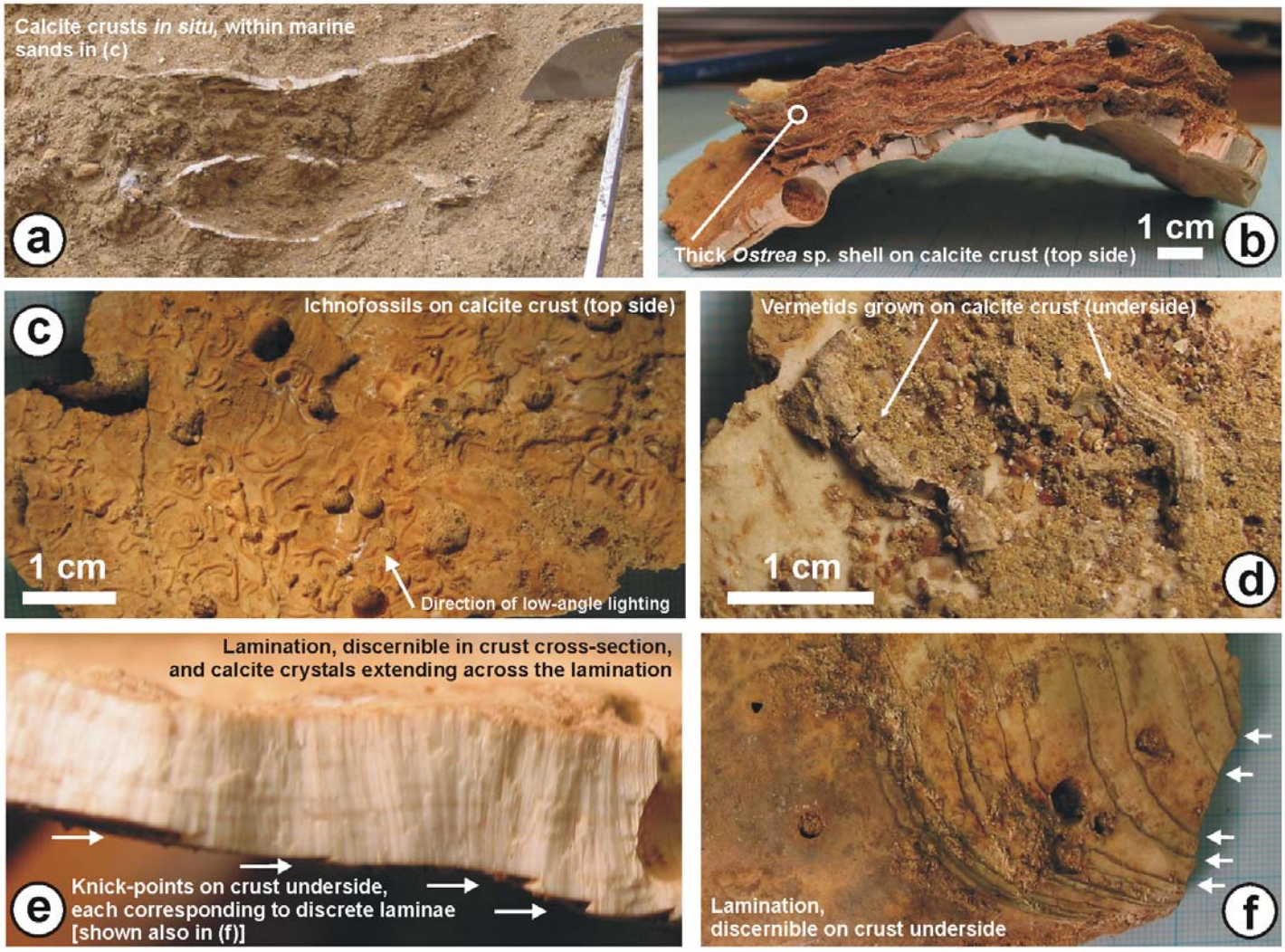
Calcite crusts *in situ*, within marine sands in (c)
a
Thick *Ostrea* sp. shell on calcite crust (top side)
1 cm
b
Ichnofossils on calcite crust (top side)
c
1 cm
Direction of low-angle lighting
Vermetids grown on calcite crust (underside)
1 cm
d
Lamination, discernible in crust cross-section, and calcite crystals extending across the lamination
Knick-points on crust underside, each corresponding to discrete laminae [shown also in (f)]
e
Lamination, discernible on crust underside
f

Fig 12

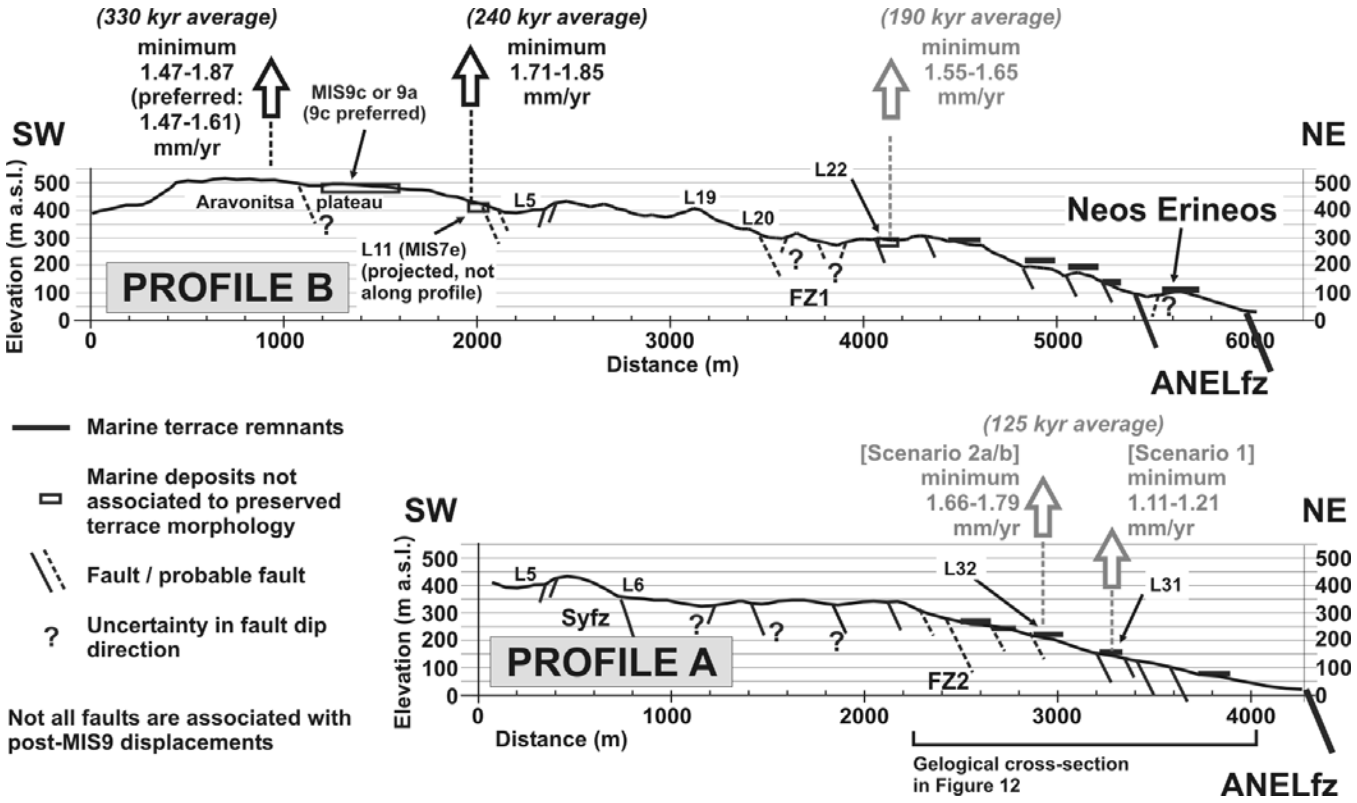
(330 kyr average)
minimum
1.47-1.87
(preferred:
1.47-1.61)
mm/yr
MIS9c or 9a
(9c preferred)
(240 kyr average)
minimum
1.71-1.85
mm/yr
(190 kyr average)
minimum
1.55-1.65
mm/yr
SW
NE
Elevation (m a.s.l.)
Aravonitsa plateau
L5
L19
L20
L22
L11 (MIS7e)
(projected, not
along profile)
FZ1
Neos Erineos
PROFILE B
Distance (m)
ANELfz
Marine terrace remnants
Marine deposits not
associated to preserved
terrace morphology
Fault / probable fault
Uncertainty in fault dip
direction
Not all faults are associated with
post-MIS9 displacements
(125 kyr average)
[Scenario 2a/b]
minimum
1.66-1.79
mm/yr
[Scenario 1]
minimum
1.11-1.21
mm/yr
SW
NE
L5
L6
L32
L31
Syfz
FZ2
PROFILE A
Elevation (m a.s.l.)
Distance (m)
Gelogical cross-section
in Figure 12
ANELfz

Fig 13

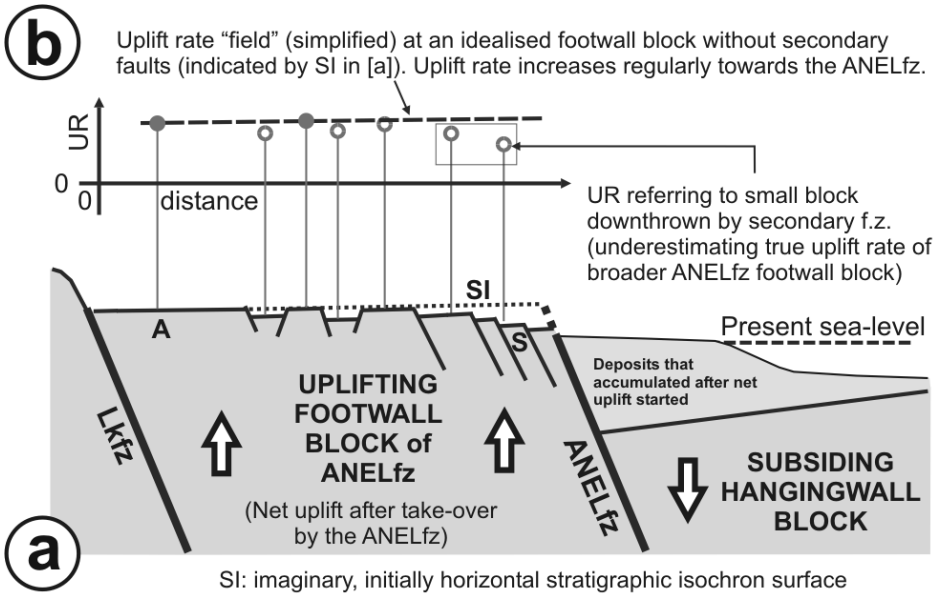
b
Uplift rate “field” (simplified) at an idealised footwall block without secondary faults (indicated by SI in [a]). Uplift rate increases regularly towards the ANELfz.
UR
0
0
distance
UR referring to small block downthrown by secondary f.z. (underestimating true uplift rate of broader ANELfz footwall block)
SI
A
S
Present sea-level
Deposits that accumulated after net uplift started
Lkfz
UPLIFTING FOOTWALL BLOCK of ANELfz
(Net uplift after take-over by the ANELfz)
ANELfz
SUBSIDING HANGINGWALL BLOCK
a
SI: imaginary, initially horizontal stratigraphic isochron surface

Fig 14